

WL-TR-94-3017

AD-A284 097



OVERVIEW OF UNSTEADY TRANSONIC WIND TUNNEL TEST ON A SEMISPAN STRAKED DELTA WING OSCILLATING IN PITCH

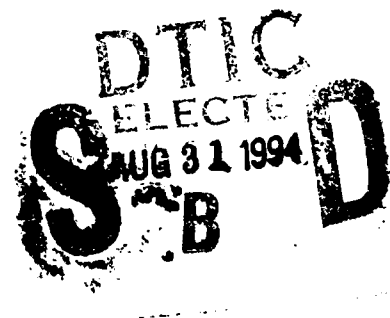
Atlee M. Cunningham, Jr.
Lockheed Fort Worth Company
Forth Worth TX

and

Ruud G. den Boer
National Aerospace Laboratory (NLR)
Amsterdam, The Netherlands

August 1994

Final Report for Period March 1989 - December 1993.



Approved for public release; distribution unlimited.

DTIC QUALITY INSPECTED 3

57PX
94-28128

Flight Dynamics Directorate
Wright Laboratory
Air Force Materiel Command
Wright-Patterson Air Force Base, Ohio 45433-7552

94 8 30 168

NOTICE

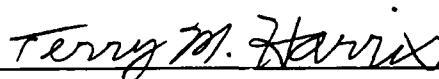
When Government drawings, specification, or other data are used for any purpose other than in connection with a definitely Government-related procurement, the United States Government incurs no responsibility or any obligation whatsoever. The fact that the Government may have formulated or in any way supplied the said drawings, specifications, or other data, is not to be regarded by implication, or otherwise in any manner construed, as licensing the holder, or any other person or corporation, or an conveying any rights or permission to manufacture, use, or sell any patented invention that may in any way be related thereto.

This report is releasable to the National Technical Information Service (NTIS). At NTIS, it will be available to the general public, including foreign nations.

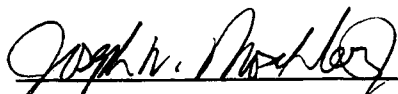
This technical report has been reviewed and is approved for publication.



LAWRENCE J. HUTTSELL
Aerospace Engineer
Aeroelasticity Section
Structural Dynamics Branch



TERRY M. HARRIS
Technical Manager
Aeroelasticity Section
Structural Dynamics Branch



JOSEPH W. MOSCHLER, MAJ, USAF
Chief, Structural Dynamics Branch
Structures Division

If your address has changed, if you wish to be removed from our mailing list, or if the addressee is no longer employed by your organization, please notify, WL/FIBG, WPAFB, OH, 45433-7542 to help us maintain a current mailing list.

Copies of this report should not be returned unless return is required by security considerations, contractual obligations, or notice on a specific document.

REPORT DOCUMENTATION PAGE			Form Approved OMB No. 0704-0188	
<small>Public reporting burden for this collection of information is estimated to average 1 hour per response, including the time for reviewing instructions, searching existing data sources, gathering and maintaining the data needed, and completing and reviewing the collection of information. Send comments regarding this burden estimate or any other aspect of this collection of information, including suggestions for reducing this burden, to Washington Headquarters Services, Directorate for Information Operations and Reports, 1215 Jefferson Davis Highway, Suite 1204, Arlington, VA 22202-4302, and to the Office of Management and Budget, Paperwork Reduction Project (0704-0188), Washington, DC 20503.</small>				
1. AGENCY USE ONLY (Leave blank)	2. REPORT DATE AUGUST 1994	3. REPORT TYPE AND DATES COVERED Final Report March 1989 - December 1993		
4. TITLE AND SUBTITLE Overview of Unsteady Transonic Wind Tunnel Test on a Semispan Straked Delta Wing, Oscillating in Pitch		5. FUNDING NUMBERS PR: 2401 TA: 02 WU: 92		
6. AUTHOR(S) Atlee M. Cunningham, Jr. and Ruud G. den Boer				
7. PERFORMING ORGANIZATION NAME(S) AND ADDRESS(ES) Lockheed Fort Worth Company Fort Worth Texas and National Aerospace Laboratory (NLR) Amsterdam, The Netherlands		8. PERFORMING ORGANIZATION REPORT NUMBER		
9. SPONSORING/MONITORING AGENCY NAME(S) AND ADDRESS(ES) Flight Dynamics Directorate Wright Laboratory Air Force Materiel Command Wright Patterson AFB OH 45433-7542		10. SPONSORING/MONITORING AGENCY REPORT NUMBER WL-TR-94-3017		
11. SUPPLEMENTARY NOTES				
12a. DISTRIBUTION / AVAILABILITY STATEMENT Approved for public release; distribution unlimited.			12b. DISTRIBUTION CODE	
13. ABSTRACT (Maximum 200 words) A wind tunnel investigation was conducted in 1992 to investigate the unsteady aerodynamic aspects of transonic high incidence flows over a simple straked wing model. This test was designed to show how low speed vortex type flows evolve into complicated shock vortex interacting flows at transonic speeds. Requirements for this test were based on a low speed test conducted in 1986 on a full span model in the NLR Low Speed Tunnel. The transonic model was a semispan version of the low speed model with some modifications. It was equipped with a three-component semispan balance to measure total wing loads, seven rows of high response pressure transducers to measure unsteady pressures and 15 vertical accelerometers to measure model motion and vibrations. The model was oscillated sinusoidally in pitch at various amplitudes and frequencies for mean model incidences varying from 4° to 48°. In addition, maneuver type transient motions of the model were tested with amplitudes of 16° and 30° total rotation at various starting angles. The test was conducted in the NLR HST in the Mach range of 0.225 to 0.90 with some preliminary vapor screen flow visualization data taken at M=0.6 and 0.9.				
14. SUBJECT TERMS unsteady aerodynamics, aeroelasticity, pressure data, transonic, high incidence flow, shock vortex interaction, force data			15. NUMBER OF PAGES 57	
			16. PRICE CODE	
17. SECURITY CLASSIFICATION OF REPORT UNCLASSIFIED	18. SECURITY CLASSIFICATION OF THIS PAGE UNCLASSIFIED	19. SECURITY CLASSIFICATION OF ABSTRACT UNCLASSIFIED	20. LIMITATION OF ABSTRACT UNCLASSIFIED	

FOREWORD

This report summarizes the results of an investigation into transonic high incidence unsteady aerodynamics. Transonic wind tunnel tests were conducted for a semispan straked delta wing model oscillating in pitch at high incidences.

This test was conducted under a cooperative program of research between the Lockheed Fort Worth Company (LFWC), Fort Worth, Texas, USA (Formerly the Fort Worth Division of General Dynamics until 28 February 1993) and the National Aerospace Laboratory (NLR), Amsterdam, The Netherlands. The test was conducted in April/May 1992. The models and corresponding support system were designed at NLR under an earlier separate program with funding from the Fort Worth Division of General Dynamics (now LFWC) and NLR. The fabrication of models, test preparation, wind tunnel test and reporting were performed at NLR under a subcontract from LFWC. This work was funded under Air Force contract F33657-84-C-0247 (CCP 4551) for the Aeronautical Systems Center, Wright-Patterson Air Force Base, Ohio. The work was administered by Mr. F. Zapata of the F-16 SPO (ASC/YPEF) and Mr. L. J. Huttshell of the Flight Dynamics Directorate of Wright Laboratory (WL/FIBG) Wright-Patterson Air Force Base, Ohio under work unit 24010292.

The program manager was Dr. A. M. Cunningham, Jr. at LFWC. The principal investigators were Dr. Cunningham at LFWC and Mr. R. G. den Boer for the wind tunnel test programs at NLR. Mr. den Boer was assisted by the following NLR specialists: C. D. G. Dogger, E. G. M. Geurts, A. P. Retel and R. J. Zwaan.

The test program for the straked delta wing will be documented in four separate reports. This report presents a general description of the model and test program and a discussion of the results. Part I will contain a description of the model, test setup, data acquisition, and data processing. Part II will contain selected test points for harmonic oscillation. Part III will contain selected data for simulated maneuvers. The three parts are listed below:

1. "Unsteady Transonic Wind Tunnel Test on a Semispan Straked Delta Wing, Oscillating in Pitch, Part I: Description of the Model, Test Setup, Data Acquisition and Data Processing," WL-TR-94-3094.
2. "Unsteady Transonic Wind Tunnel Test on a Semispan Straked Delta Wing, Oscillating in Pitch, Part II: Selected Data Points for Harmonic Oscillations," WL-TR-94-3095.
3. "Unsteady Transonic Wind Tunnel Test on a Semispan Straked Delta Wing, Oscillating in Pitch, Part III: Selected Data Points for Simulated Maneuvers," WL-TR-94-3096.

Accession For	
NTIS GRA&I	<input checked="checked" type="checkbox"/>
DTIC TAB	<input type="checkbox"/>
Unannounced	<input type="checkbox"/>
Justification	
By	
Distribution	
Availability Codes	
Avail and/or Special	

A-1

TABLE OF CONTENTS

	<u>PAGE</u>
1.0 INTRODUCTION	1
2.0 TEST OBJECTIVES	3
2.1 General Requirements	3
2.2 Specific Requirements	3
3.0 TEST SETUP	5
3.1 Wind Tunnel	5
3.2 Simple Straked Wing Model and Model Support	5
3.3 Model Instrumentation	8
3.4 Model Excitation	9
3.5 Data Acquisition System	9
4.0 PROCEDURES AND PREPARATORY TESTS	11
5.0 SIMPLE STRAKED WING MODEL TEST PROGRAM	12
6.0 TEST RESULTS AND ANALYSES	14
6.1 Low Speed Aerodynamic Characteristics of a Straked Delta Wing	14
6.2 Correlations with Full Span Model Low Speed Test Results	18
6.3 Transition from Low Speeds to Transonic Speeds	25
6.4 Steady Transonic Force and Moment Characteristics	25
6.5 Small Amplitude Oscillatory Pressure Data	30
6.6 Large Amplitude Maneuver Force and Moment Data	35
7.0 CONCLUDING REMARKS	44
8.0 REFERENCES	46

LIST OF FIGURES

<u>Figure</u>		<u>Page</u>
1	Movable, Instrumented Outboard Wing Panel and Support System	6
2	Simple Wing/Strake Configuration	7
3	Data Acquisition System	10
4	Straked Wing Model, Instrumentation, and Dynamic Support System for the Low Speed Test (Ref. 1)	15
5	Steady Force and Moment Results for Symmetric Flow, $M = 0.225$	16
6	Variation of Steady Pressure Distribution with Alpha on the Full Span Model at Low Speeds, $M = 0.225$	17
7	Comparison of the Low Speed Lift and Pitching Moment Characteristics for the Full Span and Semispan Straked Wing Models	19
8	Comparison of the Low Speed Pressures for the Full Span and Semispan Straked Wing Models	21
9	Comparison of Low Speed Strake Wing C_N and C_m	24
10	Effect of Mach Number on the Semispan Simple Straked Wing Model C_N and C_m in the NLR HST	26
11	Steady Force and Moment Characteristics for the Simple Straked Wing Semispan Model at $M = 0.9$	28
12	Unsteady Pressure Section Characteristics for Small Amplitude Oscillations, $M = 0.225$	31
13	Unsteady Pressure Section Characteristics for Small Amplitude Oscillations, $M = 0.6$	32
14	Unsteady Pressure Section Characteristics for Small Amplitude Oscillations, $M = 0.9$	33
15	Effect of Mach Number on Mean Pressure Section Characteristics	36

LIST OF FIGURES (CONTINUED)

<u>Figure</u>		<u>Page</u>
16	Effect of Mach Number on Unsteady Pressure Section Characteristics	37
17	Pitch Up/Push Over Maneuver Motion Between $\alpha = 7^\circ$ and $\alpha = 37^\circ$ for $M = 0.225$	39
18	Pitch Up/Push Over Maneuver Motion Between $\alpha = 7^\circ$ and $\alpha = 37^\circ$ for $M = 0.60$	40
19	Pitch Up/Push Over Maneuver Motion Between $\alpha = 15^\circ$ and $\alpha = 45^\circ$ for $M = 0.60$	42
20	Pitch Up/Push Over Maneuver Motion Between $\alpha = 7^\circ$ and $\alpha = 47^\circ$ for $M = 0.90$	43

LIST OF TABLES

<u>Table</u>		<u>Page</u>
1	Model Mode Frequencies	11
2	Simple Strake Wing Test Program	13

Nomenclature

b	= local wingspan, m
C_m	= wing pitching-moment coefficient, = m/QSc_r ; reference axis shown in Figure 2
C_N	= wing normal-force coefficient, N/QS
C_p	= pressure coefficient, = $(p - p_s)/Q\Delta\alpha$
$(C_p)_i$	= unsteady pressure coefficient, = $p_i/Q\Delta\alpha$ = $\text{Re}(C_p) + i\text{Im}(C_p)$
$(C_p)_m$	= mean pressure coefficient
c	= local chord, m
c_r	= reference chord, 0.821 m
f , FREQ	= frequency, Hz
i	= $\text{SQRT}(-1)$
k	= reduced frequency, = $\pi f c_r / V$
l	= wing and store rolling moment, Nm, positive wing tip up
M , MACH	= freestream Mach number
m	= wing and store pitching moment, Nm, positive nose up
N	= wing and store normal force, N, positive up
n	= store yawing moment, Nm, positive nose left
p	= pressure at model surfaces, Pa
p_s	= freestream static pressure, Pa
Q	= dynamic pressure, Pa
S	= wing area, 0.144 m^2
V	= freestream velocity, m/s
x	= chordwise coordinate, m, positive left
y	= store side force in y direction, N, positive outboard (left)
y	= spanwise coordinate, m, positive outboard (left)
z	= coordinate normal to x-y plane, m
α	= angle of attack, deg
$\Delta\alpha, d\alpha$	= amplitude of pitching motion, deg
δ	= control surface deflection, deg

Subscripts

i	= unsteady
m	= mean
MAIN	= main wing

1.0 INTRODUCTION

Steady and unsteady low speed wind tunnel tests were conducted in 1986 on a pitching simple straked wing model representative of modern fighter aircraft which make use of a strake/wing combination to achieve good high angle of attack aerodynamic characteristics (References 1 and 2). The model was oscillated in pitch at amplitudes sufficient to represent rapid pitch-ups and push-overs at dynamically scaled full scale maneuver times. Force and pressure data, as well as flow-visualization information, were obtained so that a better understanding of the developing flow fields associated with such maneuvers could be obtained. These extensive analyses, which have been documented in References 3 through 6, show how wing and strake vortices develop and interact as well as how they break down and collapse to fully stalled flows.

The interest to extend this understanding to include compressibility effects led to the consideration of another test of a similar configuration at transonic speeds. In addition, flight experience in the late 70's and early 80's with various fighter aircraft showed that limited amplitude aeroelastic oscillations (LCO) at lower angles of attack presented a serious problem by imposing further flight envelope restrictions which had not been foreseen with conventional flutter analyses and wind tunnel testing. Thus, plans were made to conduct a combined wind tunnel test using a common instrumented wing panel to investigate configurations at typical LCO flow conditions, and (2) unsteady pressures and forces for a simple straked wing under the same dynamical conditions tested at low speeds in 1986 but at increasing speeds up to the transonic regime. These planned tests, as discussed in References 7 and 8, were accomplished in September 1991 for the LCO test (Reference 8) and in May 1992 for the simple straked wing test (Reference 9).

The simple straked wing test had the straightforward objective to simply extend the understanding of flow fields at low speeds and high incidences up to transonic speeds and high incidences. The LCO test, however, had the objective of providing information that could be used to help develop a prediction method for full scale LCO characteristics of elastic aircraft. The purpose of this Part I is to present results and analyses for the simple straked wing test. In addition, analyses conducted under Lockheed Fort Worth Company funding will be summarized for purposes of providing a better understanding of the flow phenomena observed on the simple straked wing model at transonic speeds.

This part of the final report will present a brief description of the test objectives, the wind tunnel model test program as well as a selection of test results. Background for the test will first be discussed followed by descriptions of the wind tunnel models, model support, instrumentation, excitation, and data acquisition system. Next, test procedures for measuring overall loads and pressure distributions as well as the techniques used for incidence and blockage corrections will be discussed. Finally, the test program as well as test results and analysis will be presented followed by concluding remarks.

2.0 TEST OBJECTIVES

2.1 General Requirements

In order to extend to transonic speeds the understanding of low speed high incidence unsteady flow fields about an oscillating simple straked delta wing model, a wind tunnel test was planned for testing a similar configuration up to transonic speeds. This test was concerned with a semispan model of the straked wing plan form which was pitched as a single surface at large amplitudes up to maximum incidences of 50 deg. The general objectives of this test were: (1) to understand the physics of unsteady transonic vortex flows about a simple straked delta wing and; (2) to generate a steady and unsteady airloads data base for a simple straked delta wing to be used for validation of CFD computer codes.

2.2 Specific Requirements

As a means of improving the understanding of unsteady transonic vortex flows for increasing fighter maneuverability and generating a more complete airloads data base for computer code validation, a high AOA test plan was proposed in 1987 for the simple straked wing model. The test matrix was specified, but requirements included: (1) low-speed test points for determining continuity from the low-speed test of the full-span straked wing model in 1986 at NLR (Reference 1), (2) optimization of ranges of important parameters, and (3) maneuver-like model motions for selected conditions.

More recently, the low speed straked wing data base from the 1986 NLR test has been extensively investigated and a much clearer picture of the associated flow phenomena has evolved (References 3-6). Analyses of this test, which was based on a very detailed matrix of about 1200 test points, showed the importance of fine resolution of mean AOA in oscillatory testing of vortex flows. This resolution is particularly important in the vicinity of the onset of vortex bursting. In addition to force and pressure measurements, the test matrix also included flow-visualization studies from which it was possible to define the three-dimensionality of the vortex structure and how its changes were related to changes in the forces and surface pressures.

In August 1988, a flow-visualization test was conducted at NASA Langley in which transonic shock/vortex interaction was investigated on a 50 deg swept clipped delta wing. Subsequent analyses of these results showed that the vortex structure was significantly altered at transonic speeds and that normal shock interaction with the vortex further complicated an already complex phenomenon. Similar to the low speed tests, definition of the three-dimensional nature of the shock/vortex interaction would be required in order to better understand flow field effects on forces and surface pressures.

These investigations have repeatedly shown the importance of adequate flow visualization and fine resolution in the variation of such parameters as Mach and incidence in the testing of separated flows. This is particularly true at transonic speeds where shock induced separation and vortex flows are dominant and the flow fields are highly three dimensional. Also, since 1987, NLR had acquired added capabilities that permitted a meaningful restructuring of the test programs originally proposed in 1987. These added capabilities included: (1) remote control of mean angle of attack for dynamic testing at transonic speeds; (2) a new dynamic data recording system; and (3) adaptation of the water vapor/laser light sheet flow-visualization technique developed at NASA Langley.

In adapting the water vapor/laser light sheet flow-visualization technique developed at NASA Langley, NLR conducted several tests at transonic speeds using an existing generic straked wing model, all under NLR funding. These preliminary tests gave excellent flow-visualization results for steady transonic vortex flows using still photography. For dynamic flows, NLR planned to use a high speed CCD video camera.

As a result of the above considerations, a more extensive test matrix was planned for the simple straked wing wind tunnel test. This expanded matrix resulted in nearly 700 runs which included sufficient Mach number, mean angle, motion amplitude and frequency variations to establish how the low speed characteristics that were identified in the 1986 test data base evolved into the shock/vortex interactions at transonic speeds. Continuity between the 1986 low speed test and this transonic test were quantified and maneuver-like model motions were also performed for selected conditions. Because of the importance of flow-visualization, NLR also conducted additional testing with the water vapor/laser light sheet technique at selected conditions under their own funding in order to establish feasibility of this approach for obtaining meaningful dynamic flow visualization data at transonic speeds.

3.0 TEST SETUP

Detailed information on the test setup at NLR is provided in Part II of this final report. The following is a summary of that information.

3.1 Wind Tunnel

The simple straked wing test was conducted in the NLR 2.0 x 1.6 m² high-speed wind tunnel situated in Amsterdam. The tunnel has a closed circuit with a test section length of about 2.5 m. The test section can accommodate either sting or sidewall mounted models. Sidewall mounting was used for the semispan model in the current test. The tunnel has a Mach range of 0.3 to 1.2 and a maximum Reynolds number of 22×10^6 per meter at $M = 0.95$. Variable pressure and temperature capability provides close control of Reynolds number as well as Mach number.

3.2 Simple Straked Wing Model and Model Support

The wing panel with basic instrumentation is shown schematically in Figure 1. Support was provided through a semispan balance beam which was in turn supported by bearings mounted on the sidewall turntable. The hydraulic actuator, also mounted on the turntable, provided the oscillatory pitching excitation of the wing panel. Model mean angle-of-attack was then controlled through positioning of the sidewall turntable independent of the hydraulic actuator position.

The wing panel was of a "clam-shell" design so that all instrumentation inside the wing was accessible. It was fabricated of high-strength aluminum alloy so as to minimize inertia loads and has instrumented leading and trailing edge flaps whose positions were varied by changing the attachment brackets. Instrumentation is described in Section 3.3.

The simple strake configuration is shown in Figure 2. Since this test was a transonic counterpart to the low speed test of a simple straked wing (Reference 1), the strake section also moved with the wing and was, therefore, attached to the basic wing panel. Loads from both the wing and strake were carried through the semispan balance beam. The leading and trailing edge flaps could not be deflected.

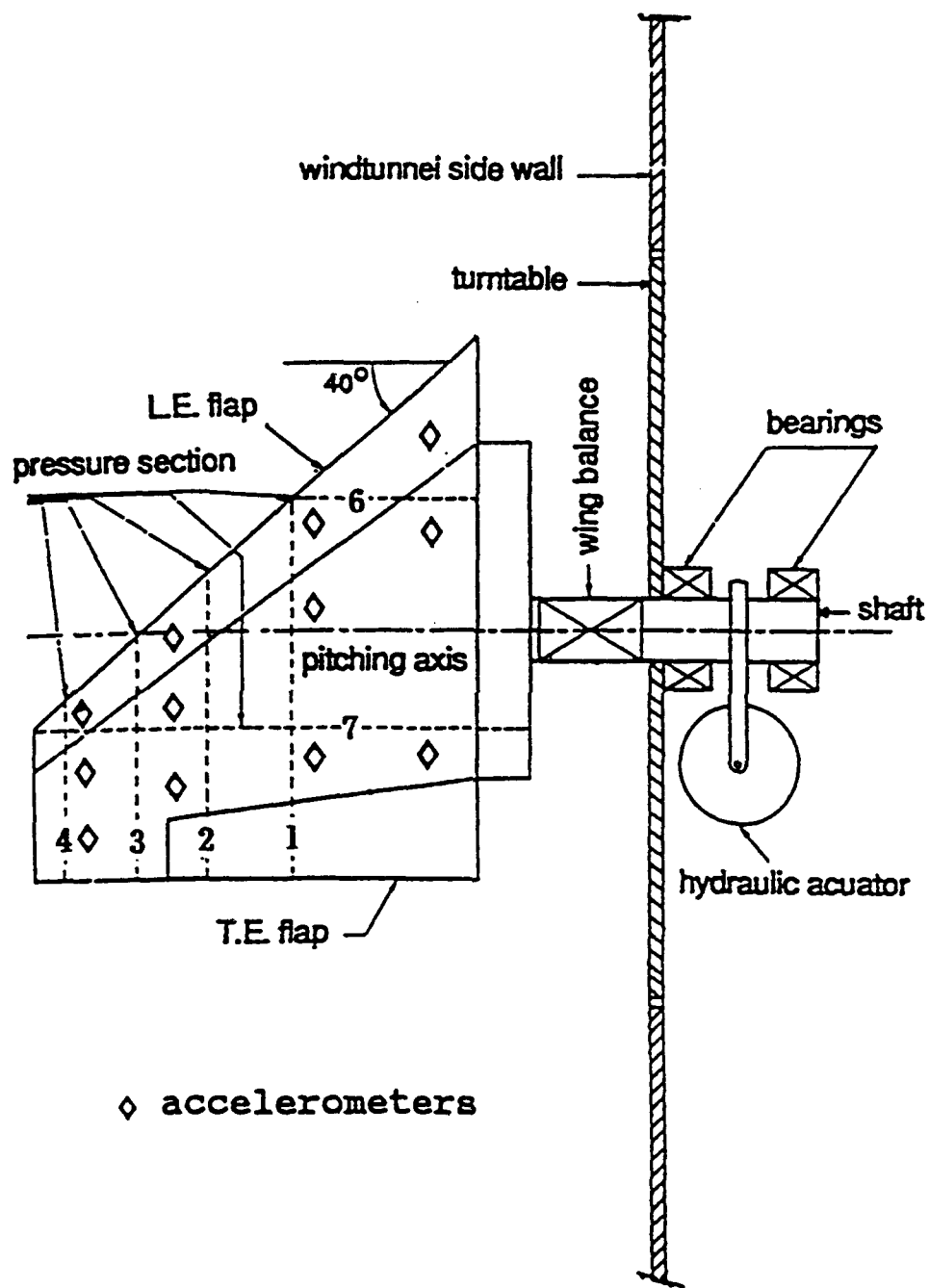


Figure 1 Movable, Instrumented Outboard Wing Panel and Support System

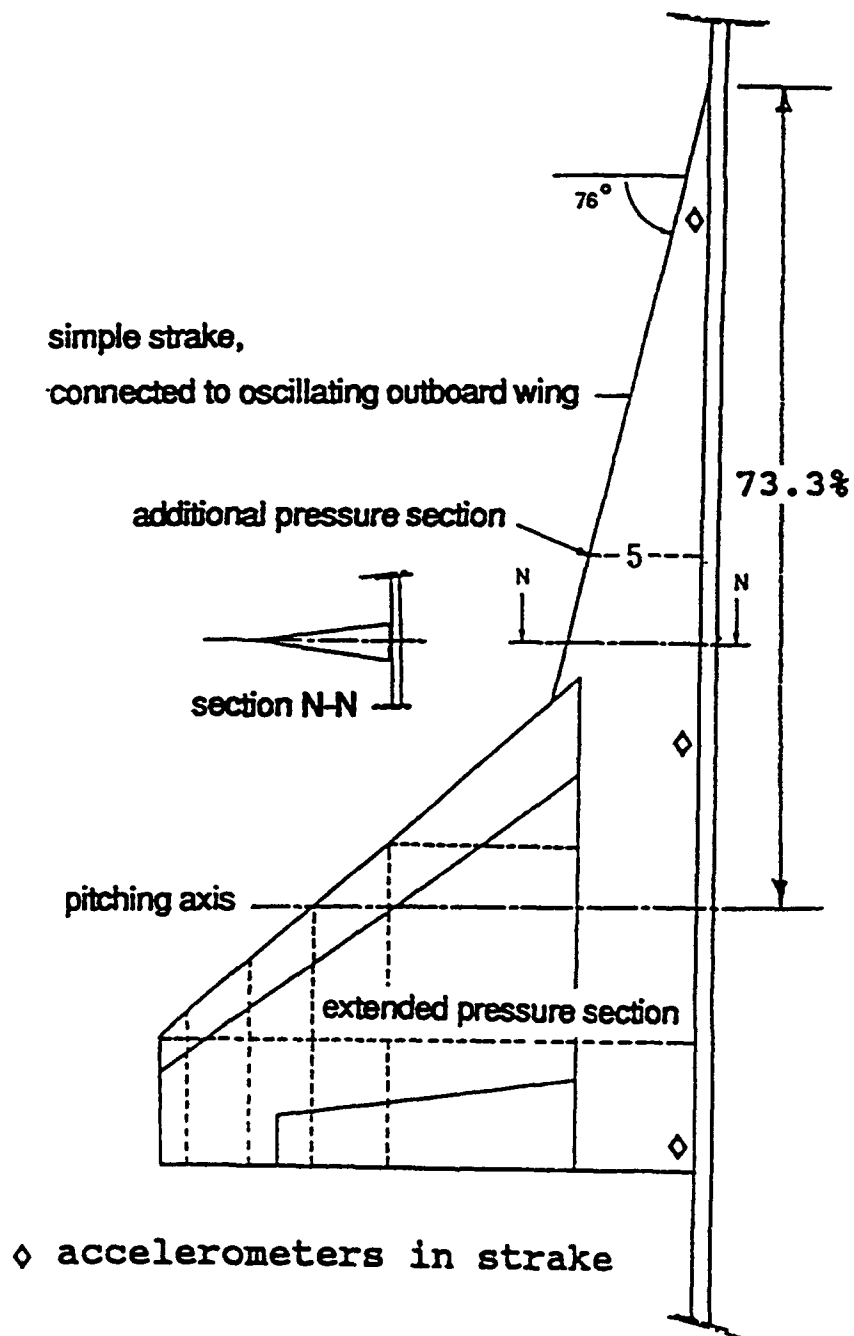


Figure 2 Simple Wing/Strake Configuration

All model and support system parts were designed and fabricated by NLR at the Amsterdam and Noordoostpolder facilities. The instrumentation and calibration were also accomplished by NLR.

3.3 Model Instrumentation

The model instrumentation consisted of a main wing semispan balance, a dynamic incidence transducer, in situ pressure transducers, and accelerometers. In addition, temperature and reference pressure transducers were provided in the model. Locations of instrumentation are indicated in Figures 1 and 2.

The three component main wing balance was designed to provide adequate stiffness and strength and yet retain sufficient sensitivity for accurate aerodynamic loads measurements. Specifically, this balance measured normal force, rolling (or bending) moment and pitching moment.

A linear variable differential transducer (LVDT) was mounted between the beam balance and the support to measure the oscillation amplitude input to the model. Mean incidence of the model was measured by a very sensitive accelerometer attached to the sidewall turntable.

The pressure transducers were mounted such that they were electrically isolated, free of local model deformations, and not influenced by model accelerations. Four chordwise and two spanwise rows were located as shown in Figure 1 for a total of 87 pressure transducers. The two inboard chordwise rows contained both upper and lower transducers with more on the upper surface. All pressure rows extended onto the leading and trailing edge flaps. Grouping toward the wing tip was done in order to concentrate instrumentation in the regions of known shock induced separation as well as leading edge separation at transonic speeds and low incidence. Pressures on the forward strake were measured with an additional spanwise row (Section 5) with 10 pressure transducers as shown in Figure 2. The sensitivity of the pressure transducers showed a small variation with temperature. By measuring the model temperature with a thermistor, the correct sensitivity of the pressure transducers could be selected for processing recorded electrical signals into pressure data.

Vertical accelerometers were also located at 12 positions on the wing as shown in Figure 1 and at 3 positions on the strake section as shown in Figure 2.

3.4 Model Excitation

Excitation was provided by an electro-hydraulic shaker system which consisted of a hydraulic power supply, a combined linear actuator and servo valve, and a feedback control unit (Reference 10). The hydraulic actuator was mounted on the sidewall turntable. The piston was connected to a crank on the balance beam (see Figure 1) to convert from linear to rotational motion. Design amplitude limitations for the simple straked wing configuration were ± 2.0 deg at 16 Hz. Motions during the simple straked wing test were both sinusoidal and transient maneuvers.

3.5 Data Acquisition System

The wind tunnel test was performed using a computer controlled data acquisition system (see Figure 3) called PHARAO (Processor for Harmonic and Random Oscillations), which is capable of sampling 128 (time) signals simultaneously.

The electrical signals of the instruments were first amplified in the Multichannel Conditioning Units (MCCUs) with 128 channel capacity and a separation was made between ac and dc. The ac signals were filtered (for antialiasing), sampled by the ac converter and stored on an optical disc. One oscillator was used to control both the hydraulic actuator (see Section 3.4) as well as the sampling of the electrical signals, to have perfect synchronization. Sample frequencies and filter settings were chosen proportional to the driving frequency of the mode. In most cases, 4096 samples were recorded for each channel with a frequency of 32 times the frequency of the model motion, so 128 full cycles of the first harmonic were recorded. For quick look presentation, the time traces were averaged using Phase Locked Time Domain Averaging (PLTDA) and Fourier transformed to harmonic components. The balance loads were corrected for inertial loads and the influence of temperature on pressure transducer sensitivity was accounted for.

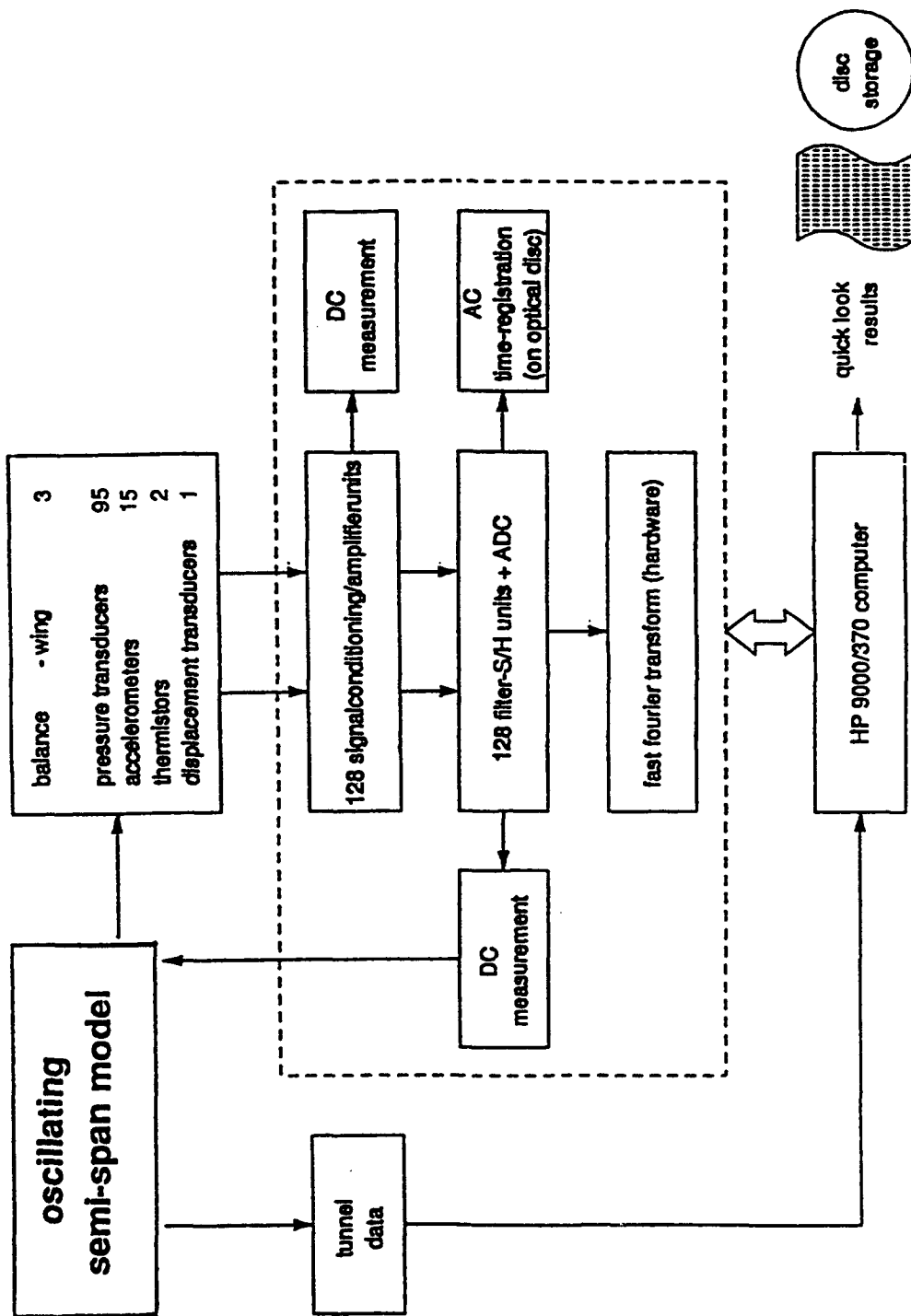


Figure 3 Data Acquisition System

4.0 PROCEDURES AND PREPARATORY TESTS

Detailed information on procedures and preparatory tests at NLR is provided in Part II of this final report. The following is a summary of that information.

The main objective of these measurements was to establish the relationship between the mechanical motion of the model as input and the pressures, forces, and moments as output as measured by the model instrumentation. Using the data acquisition system (Section 3.5), the relationship was established through determination of the zeroth (mean) and the first eight harmonics of the measured output signals. All data quantities were normalized into standard coefficient form using model motion and wind tunnel aerodynamic quantities for the normalization terms. In most cases, about 1 minute was required per test point at a given mean angle, frequency, and amplitude. All data reduction was performed on the HP 9000/370 computer and all results including time histories were stored on disks for later analyses.

Wing incidence was influenced by structural deformations of the balance and wing panel. Thus, mean wing position was adjusted with the hydraulic actuator system for each mean angle-of-attack setting. This correction was less than 0.1 deg for the maximum design aerodynamic pitching moment applied to the wing. No additional incidence or blockage corrections due to wind tunnel wall presence were used for this test.

Model vibration modes, frequencies, and masses were needed for calculating inertia corrections to the various balance measurements. Thus, vibration tests were conducted on the model for all possible wing store configurations. Frequency ranges for the primary wing modes for all configurations are shown in Table 1. Flutter analyses were also performed with the measured model modes, frequencies, and generalized masses using linear theory (doublet lattice) unsteady aerodynamics. Results indicated that flutter speeds were more than twice the testing speeds.

TABLE 1 MODEL MODE FREQUENCIES

Balance Pitch Mode	91.20 Hz
1st Spanwise Bending Mode	136.30 Hz
1st Wing Tip Torsion Mode (Local)	166.48 Hz

5.0 SIMPLE STRAKED WING MODEL TEST PROGRAM

The simple straked wing model was tested at three Mach numbers. Runs at $M = 0.225$ were conducted to establish continuity between the semispan model in the HST with the full span model in the NLR LST (1986, Reference 1). Runs at $M = 0.60$ were conducted to obtain data at an intermediate speed to study the change in vortex flows with increasing compressibility effects without the presence of shocks. Finally, runs at $M = 0.90$ were made to obtain data with shock vortex interactions. All three Mach numbers were tested at a Reynolds number of 8.0×10^6 based on the strake root chord.

The nominal test program for the oscillating model is shown in Table 2. The larger amplitudes denoted by * were tested only during the transient maneuver motion portion of the test. This test program was used as a guide, however, the actual matrix tested was much denser where extra points were added according to trends observed at the various Mach numbers. Mean data points were obtained with small amplitude oscillations at low frequency for mean angular increments of no greater than 2 deg but usually 1 deg for each Mach number up to the maximum angle tested. A detailed run schedule for the simple straked wing oscillatory test program is given in Part II of this final report.

Special runs were made at $M = 0.225$ where the tunnel was evacuated to achieve a Reynolds number of 3.7×10^6 (based on strake root chord) which matched the 1986 low speed test Reynolds number in Reference 1. At $M = 0.90$, a series of incidences was tested at a Reynolds number of 14.0×10^6 , otherwise all tests were conducted at the baseline value of 8.0×10^6 .

Initial tests at $M = 0.225$ were conducted with and without a filler plate installed on the model (see Part II of this final report for more detail). The purpose of the filler plate was to reduce the gap between the strake root and the wind tunnel wall from 7mm to 2mm. Results with the filler plate installed provided a better match with the full span test data of Reference 1 as will be discussed in more detail in the next section. Thus, it was decided to perform all other test points (data point numbers greater than 60) with the filler plate installed.

The maneuver like transient runs were made at all three Mach numbers for amplitudes of 8 deg and 16 deg at 3.8 Hz. Maximum angles for the dynamic motions were 50 deg for $M = 0.225$, 46 deg for $M = 0.60$, and 38 deg for $M = 0.90$. A detailed run schedule for the simple straked wing maneuver test program is given in Part II of this final report. Four maneuver types

were conducted at each test condition: (1) pitch-up and hold from minimum α to maximum α ; (2) pitch-down and hold from maximum α to minimum α ; (3) pitch-up/pitch-down from minimum α to maximum α back to minimum α ; and (4) pitch-down/pitch-up from maximum α to minimum α back to maximum α .

TABLE 2 SIMPLE STRAKE WING TEST PROGRAM

M	Mean α Values				
	α_1	α_2	α_3	→	α_{MAX}
0.3	6°	10°	14°	→	48°
0.6	6°	10°	14°	→	46°
0.9	6°	10°	14°	→	30°

f, d α matrix:

f (Hz)	d α (deg)			
4			8*	16*
6	0.5	4	8	
8	2	4	8	
12	2			
16	2			

* Maneuver-like model motions (1-cos) for selected mean α values.

6.0 TEST RESULTS AND ANALYSES

The purpose of testing the simple straked wing at transonic speeds was to obtain information which would provide for a better understanding of how shock and vortex interactions evolve at high subsonic speeds and high incidences. Since the basis for this understanding is the characteristics at low speeds where shocks are not present in the flow fields, it is important that discussions begin with those characteristics.

6.1 Low Speed Aerodynamic Characteristics of a Straked Delta Wing

A low speed test of the full span straked wing model was conducted at NLR in 1986 (References 1-6). This model was instrumented for force and unsteady pressure measurements. Incidences from -8 deg up to 50 deg were tested with the model both stationary and oscillating in pitch at either 0 deg or ± 5 deg sideslip. Amplitudes of oscillation ranged from ± 2 deg to ± 18 deg. The Mach number was constant at $M = 0.225$ with a Reynolds number of 3.7×10^6 based on the root chord. The model, instrumentation, and dynamic support system are shown in Figure 4.

The variations of steady normal force, C_N and pitching moment, C_m with angle of attack, α , are shown in Figure 5 for zero sideslip. Important flow field characteristics and transitions are also denoted where the "sections" referred to in those notations are the pressure transducer rows shown in Figure 4. Corresponding steady pressure data for all four sections are shown in Figure 6 for $\alpha = 10$ deg, 19 deg, 22.4 deg, 36 deg, and 42.3 deg. The pressure data were chosen to highlight various flow regimes and transitions.

The "Linear" range of aerodynamic force development is clearly evident in Figure 5 in both the C_N and C_m data from $\alpha = -8$ deg to 8 deg. Beyond 8 deg, the C_N and C_m curves show an upward change in slope that is indicative of the development of vortex flows over both the wing and strake. This is illustrated by the pressure data and sketch of vortex structure in Figure 6 at $\alpha = 10$ deg for pressure Section 2. The small peak at $2y/b = 0.45$ is produced by the strake vortex and the stronger peak at $2y/b = 0.8$ by the wing vortex.

The vortex flow range continues to develop until $\alpha = 18$ deg and 19 deg where a distinct break occurs in the C_N and C_m data. This break signals the onset of vortex burst which represents the limit of vortex strength that can be maintained by the flow fields. Bursting tends to occur simultaneously for the wing and strake vortices when the two merge. The pressure data and sketch

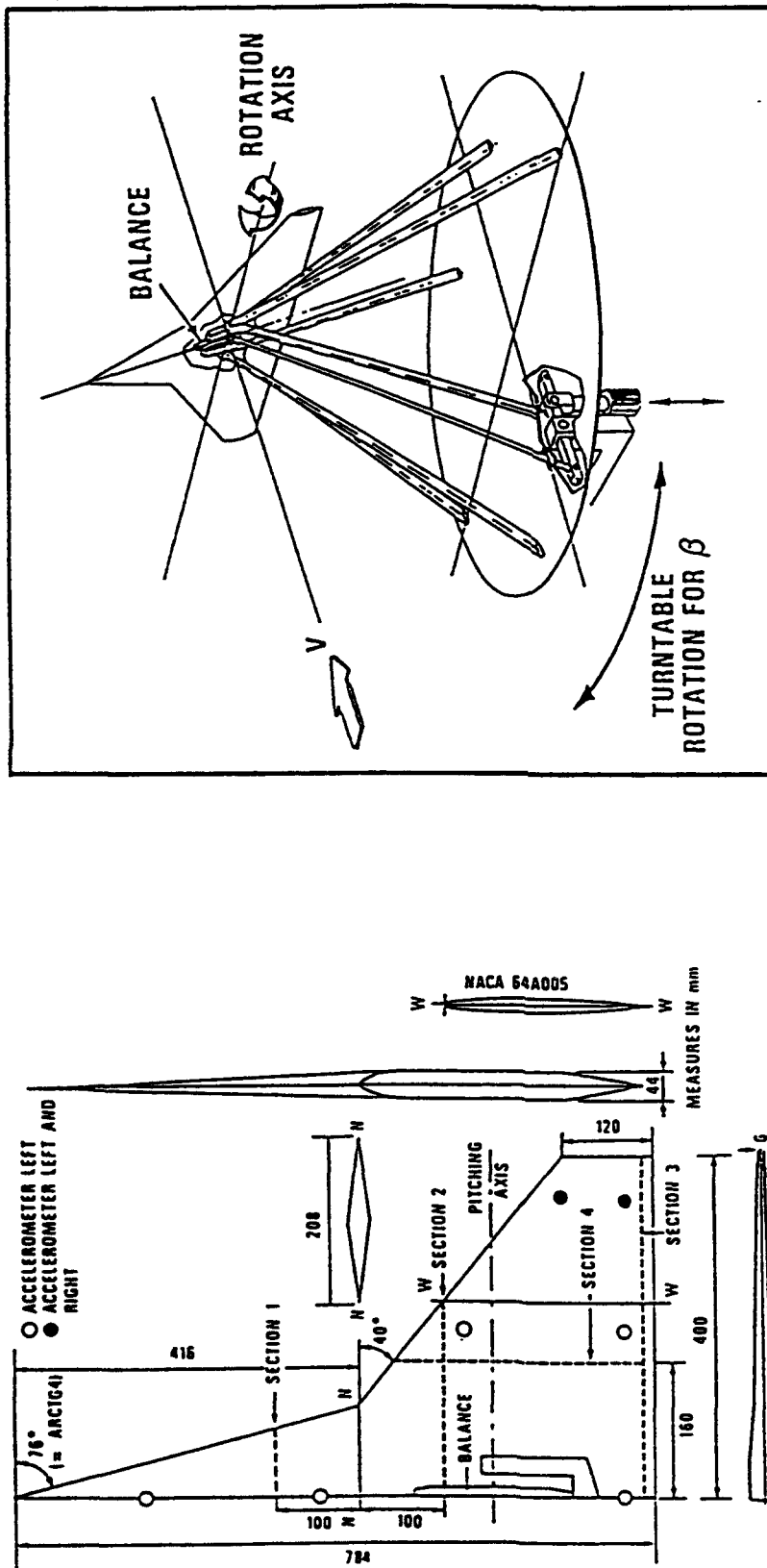


Figure 4 Straked Wing Model, Instrumentation, and Dynamic Support System for the Low Speed Test (Reference 1)

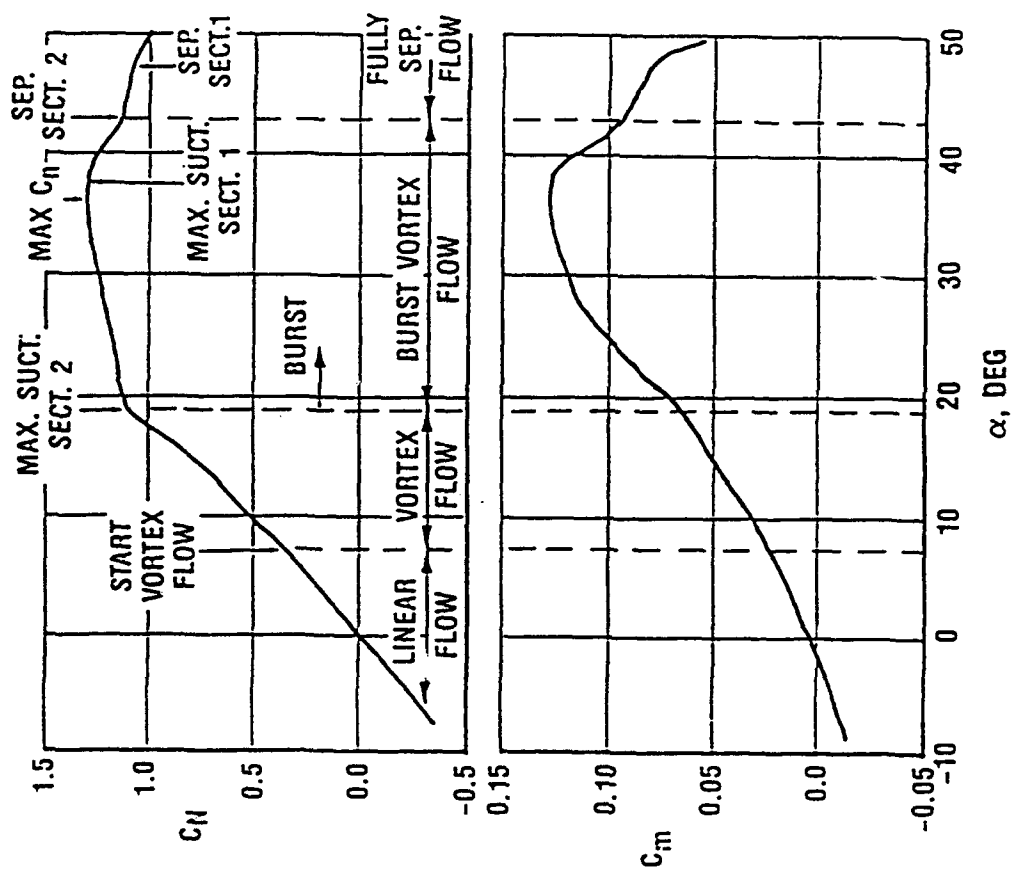


Figure 5 Steady Force and Moment Results for Symmetric Flow, $M=0.225$

of burst vortex structure for $\alpha = 19$ deg in Figure 6 show well developed vortices at both the forward pressure sections (1 and 2) but a deterioration of pressure recovery on the out-board half of the trailing edge section (3).

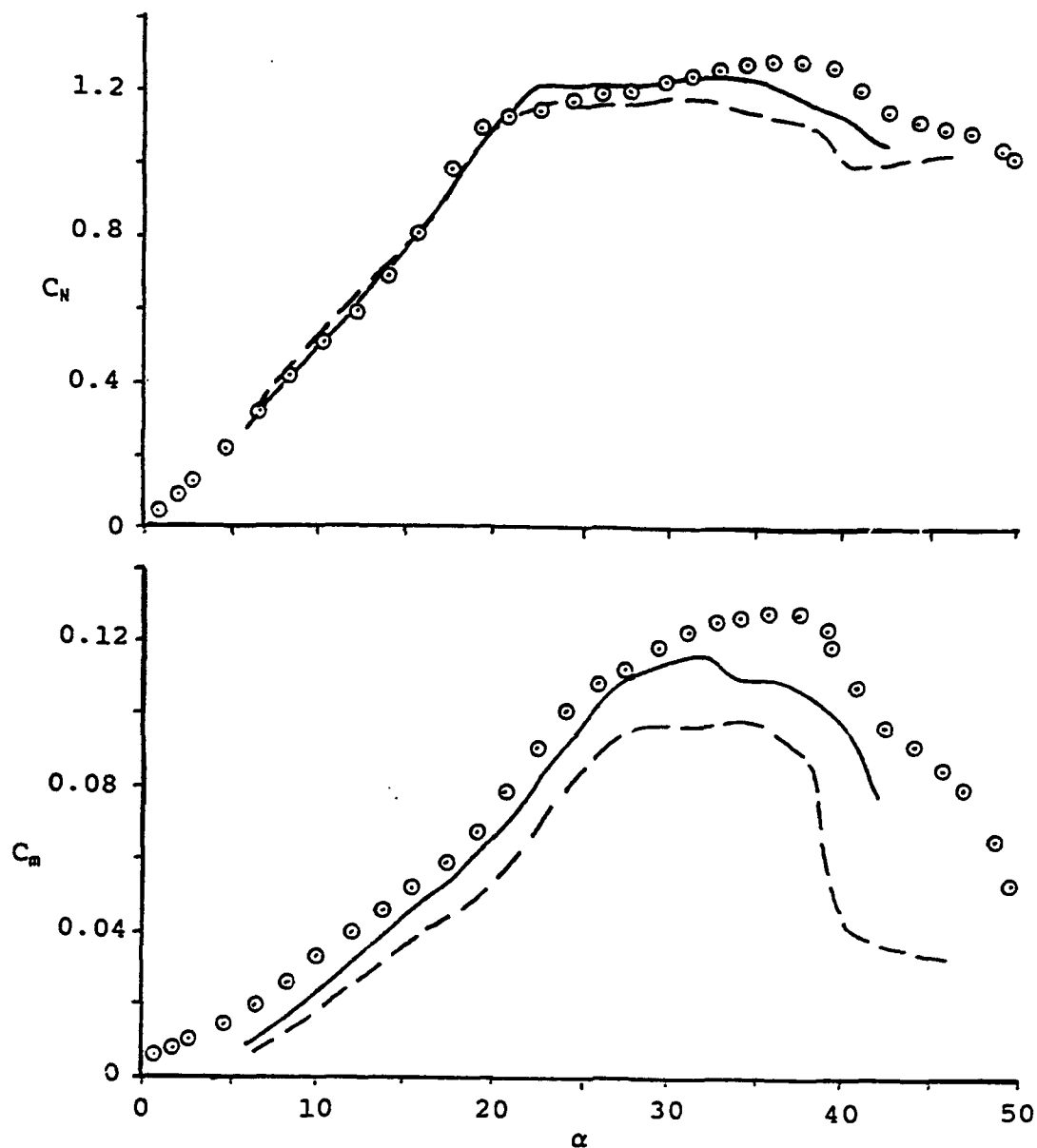
For increasing α in the burst vortex regime, the strake vortex strength increases but the burst point continues to move forward. These opposing trends result in a much lower slope in the C_N curve as shown in Figure 5, however, the slope is almost constant from $\alpha = 19$ deg to about 34 deg. The gain in lift forward, due to strake vortex strength increase, and the loss in lift aft, due to vortex burst forward movement, produces a pitch-up in the C_N curve as shown in Figure 5. The pressure data and sketches of burst vortex development in Figure 6 for $\alpha = 19$ deg, 22.4 deg, and 36 deg show the deterioration of the wing vortex strength at Section 2 and the continued increase of the strake vortex strength up to 36 deg at Section 1.

Beyond the maximum value of C_N at $\alpha = 36$ deg the flow over the entire wing and strake rapidly collapses to completely separated or flat plate flow. Under these conditions for increasing α the normal force is falling off and the center of pressure is moving toward the geometric centroid of the planform as indicated by a rapid decrease in pitching moment. The pressure data at $\alpha = 42.3$ deg in Figure 6 show that the pressure distributions are nearly flat at about the same level for all sections except Section 1 on the strake. At this angle, the strake vortex burst has progressed forward of Section 1 as shown in the sketch for $\alpha = 42.3$ deg.

6.2 Correlations With the Full Span Model Low Speed Test Results

Since the straked wing model was to provide a transonic extension to the low speed test (Reference 1), the first step was to correlate force, moment, and pressure data for the two models at the same test conditions of $M = 0.225$ and $R_e = 3.7 \times 10^6$ (based on root chord). Besides being a semispan model, the transonic model also had some wing twist (nose down 2.5 deg at the wing tip), a thinner wing section (NACA 64A004 as compared to NACA 64A005 for the low speed model) and an underwing thickening to house the semispan three component balance.

Lift and moment coefficients from the low speed full span test in the NLR LST of Reference 1 and the low speed semispan test in the NLR HST, are shown in Figure 7. The two sets of semispan results are for the model with and without the 5mm filler plate as was discussed previously in Section 5.0. The gap between the model root and wind tunnel wall was 2mm with the filler plate installed and 7mm without. As can be seen, installation of the filler plate improved both the lift and moment trends with incidence



$$M = 0.225, R_e = 3.8 \times 10^6$$

- (LST) \circ Full Span Model (Low Speed Test, Reference 1)
 (HST) ——— Semispan Model (With Filler Plate, Wall Gap=2mm)
 (HST) ---- Semispan Model (Without Filler Plate, Wall Gap=7mm)

Figure 7 Comparison of the Low Speed Lift and Pitching Moment Characteristics for the Full Span and Semispan Straked Wing Models

although the correlation is not perfect. The largest deficiencies occur above incidences of about 30 deg.

A comparison of pressure data on the two models actually provides a better assessment of model differences as shown in Figures 8(a), (b), and (c). Pressure comparisons are made along the two spanwise rows, Section 5 on the strake and Section 6 on the wing for the semispan model (see Figures 1 and 2) which correspond to Sections 1 and 2, respectively, on the full span model (see Figure 4). In Figure 8(a), the semispan results with and without the filler plate are essentially the same but show a lower vortex strength development. In Figure 8(b), effects of the filler plate are more apparent where vortex peaks described by that corresponding set of data are much closer to the peaks described by the full span model test pressures. The semispan model strake vortex, however, is still weaker. The weaker strake vortex on the semispan model is attributed to the counter rotating vortex that exists in the corner formed by the wing upper surface and wall intersection. This effect is characteristic on semispan models and is directly influenced by the wind tunnel wall boundary layer characteristics. Variation of the model/wall gap size with the filler plate was included in this test primarily because of the concerns for this corner flow effect. By allowing just enough gap, this corner vortex could be weakened so as to have minimal effect. Too much gap would augment the corner vortex and significantly weaken the strake vortex and/or push it more outboard as seen in Figure 8(b).

Results in Figure 8(c) correspond to maximum normal force ($\alpha = 32$ deg and 37 deg) and fully stalled flows ($\alpha = 42$ deg and 47 deg) on the semispan and full span models. Flow breakdown begins at a lower incidence on the semispan model, especially without the filler plate. However, at $\alpha = 32$ deg on the strake (Section 5), a high suction is seen near the semispan model root which appears to be a second vortex peak. It is suspected that this peak is caused by the counter rotating corner vortex created in the wing-wall junction by the high velocity vertical flow between the model root and the wind tunnel wall as discussed above. In fully stalled flow ($\alpha = 42$ deg and 47 deg), the semispan model section levels are slightly lower than those of the full span model, however, the differences are small.

Since the semispan model was tested at a constant Reynolds number of 8.0×10^6 for increasing Mach number from 0.225 to 0.9, a comparison of the semispan low speed data at $R_e = 8.0 \times 10^6$ and the full span data at $R_e = 3.7 \times 10^6$ is shown in Figure 9. Three differences are noticed. First, vortex bursting occurs at a higher angle on the semispan model at 22 deg than on the full span model of 19 deg. This difference is primarily attributed to wing tip twist. Second, the maximum value of C_N occurs at 31 deg on the semispan model but at 36 deg on the full span model. This influence is attributed to the semispan effect where wall



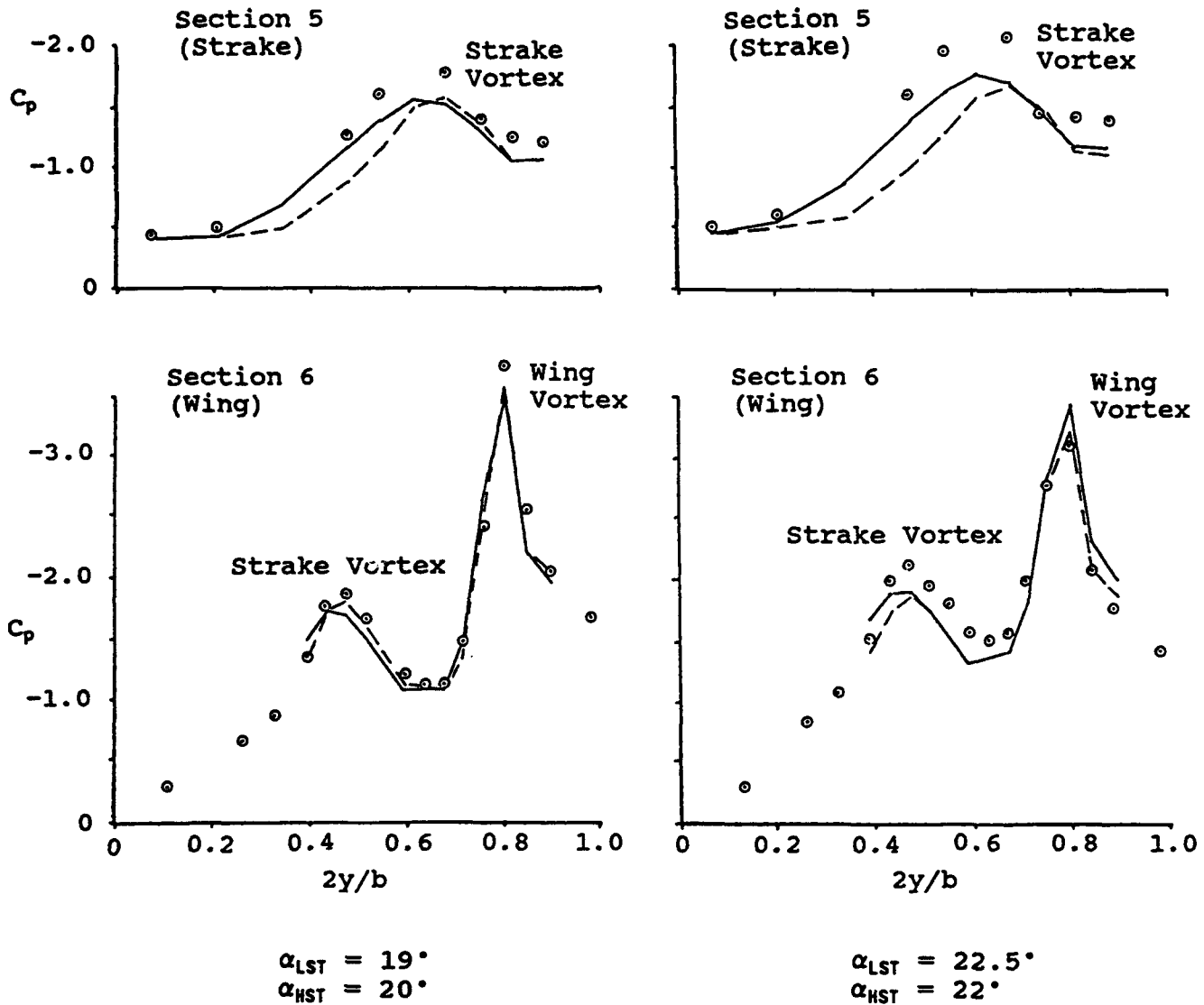
$$\alpha = 8^\circ$$

$$M = 0.225, R_e = 3.8 \times 10^6$$

- (LST) \circ Full Span Model (Low Speed Test, Reference 1)
 (HST) — Semispan Model (With Filler Plate, Wall Gap=2mm)
 (HST) ---- Semispan Model (Without Filler Plate, Wall Gap=7mm)

Figure 8 Comparison of the Low Speed Pressures for the Full Span and Semispan Straked Wing Models

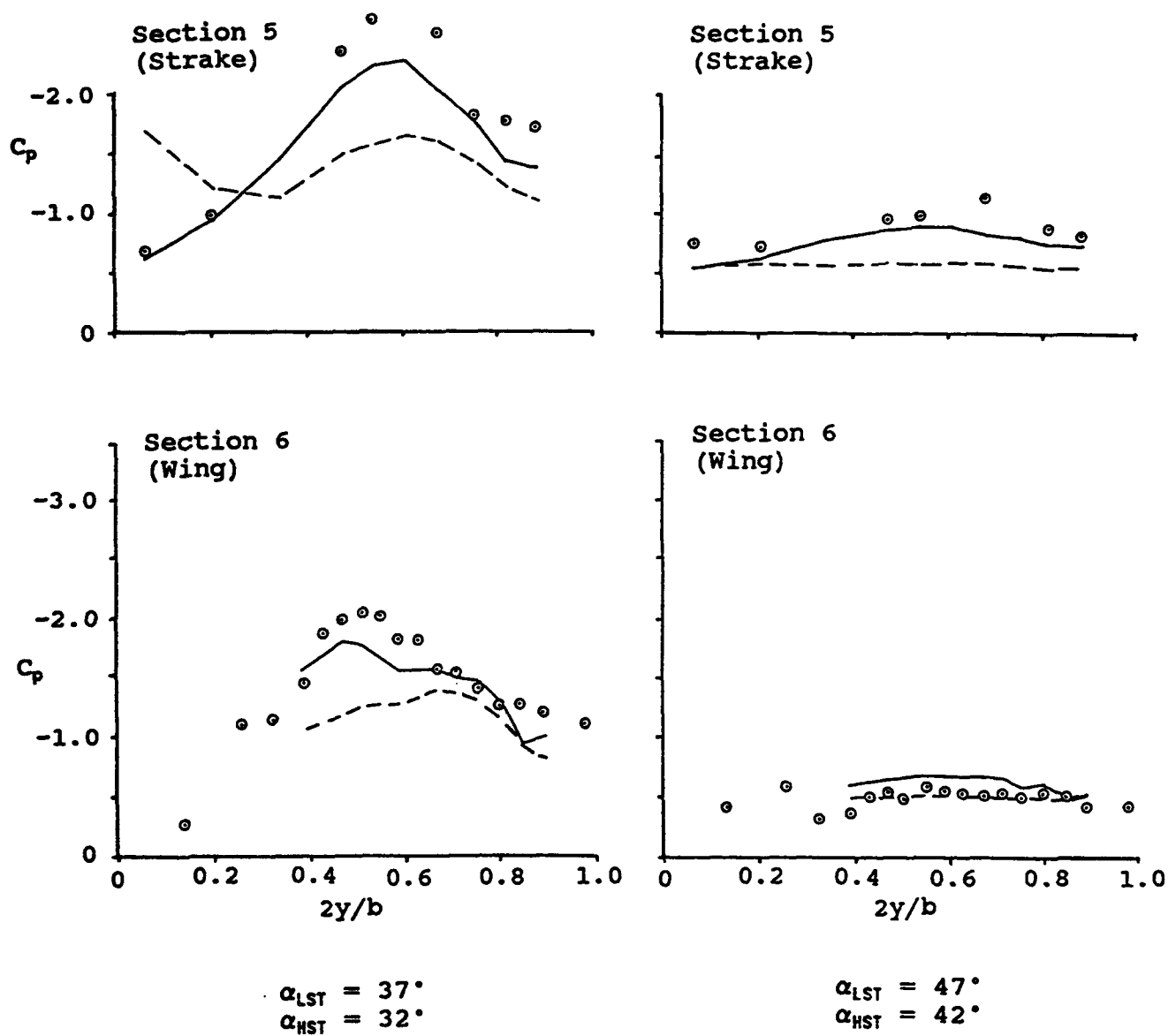
(a) Low Incidence



$$M = 0.225, R_e = 3.8 \times 10^6$$

- (LST) \circ Full Span Model (Low Speed Test, Reference 1)
 (HST) — Semispan Model (With Filler Plate, Wall Gap=2mm)
 (HST) ---- Semispan Model (Without Filler Plate, Wall Gap=7mm)

Figure 8 (b) Vortex Bursting



$$M = 0.225, R_e = 3.8 \times 10^6$$

- (LST) \circ Full Span Model (Low Speed Test, Reference 1)
(HST) — Semispan Model (With Filler Plate, Wall Gap=2mm)
(HST) ---- Semispan Model (Without Filler Plate, Wall Gap=7mm)

Figure 8 (c) Flow Breakdown

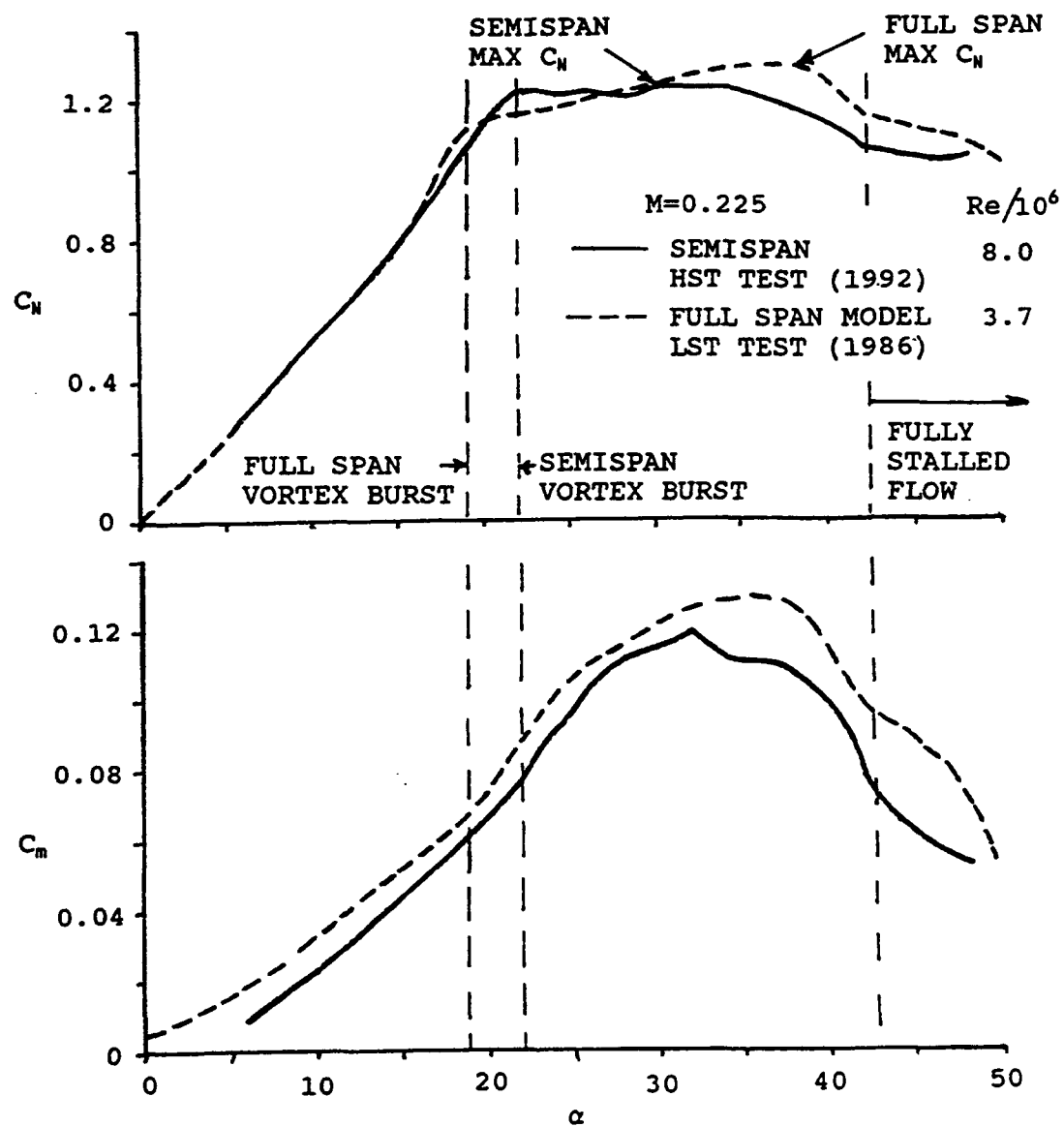


Figure 9 Comparison of Low Speed Strake Wing C_N and C_m

boundary layer weakens vortical flows at high angles as was discerned from pressure data comparisons above. Third, the maximum value of C_m is lower for the semispan model which is also attributed to semispan effects. Fully stalled flow, however, seems to develop at about 42 deg for both models.

Although the exact points for critical flow transitions do not completely match for the two models, the trends are very similar indicating that the important flow mechanisms are preserved on the semispan model. Thus, it should then be possible to identify how the flow fields evolve with increasing compressibility effects.

6.3 Transition from Low Speeds to Transonic Speeds

Results for the semispan model are shown in Figure 10 for $M = 0.225$, 0.6 , and 0.9 for a Reynolds number of 8×10^6 . All three C_m curves are very similar with exception of (1) the higher slope at $M = 0.9$ and $\alpha < 10$ deg and (2) the higher peak at $\alpha \approx 24$ deg for $M = 0.6$. The C_m curves are also very similar but show the typical aft movement of the center of pressure with increasing Mach.

With exception of the unique features at $M = 0.9$, $\alpha < 10$ deg and $M = 0.6$, $\alpha \approx 24$ deg, all trends are very similar indicated that the major flow field characteristics and transitions are also either comparable or similar. Linear flow appears to exist up to about 8 deg or 10 deg at all three Mach numbers. Vortex flow seems to dominate up to 22 deg ($M = 0.225$), 24 deg ($M = 0.6$), and 19 deg ($M = 0.9$) where some type of vortex burst or flow breakdown occurs. The pitchup tendency beginning with the breakdown onset is common to the three speeds and is terminated with a flat characteristic at $M = 0.6$ and 0.9 . This pitchup is mostly due to loss of lift at the trailing edge and outboard regions as indicated by pressure data. Although vortex bursting is dominant at $M = 0.225$ and 0.6 , it is not clear what is occurring at $M = 0.9$ as will be discussed later.

The plateau regions of lift and moment are very similar indicating that flow deterioration is occurring simultaneously over the entire wing at the three speeds. Finally, total stalling appears to begin at about 35 deg and is fully developed by about 42 deg for all three Mach values.

6.4 Steady Transonic Force and Moment Characteristics

Extensive analyses were conducted under Lockheed Fort Worth Company funding on pressure data and some preliminary flow visualization data both obtained during the simple straked wing

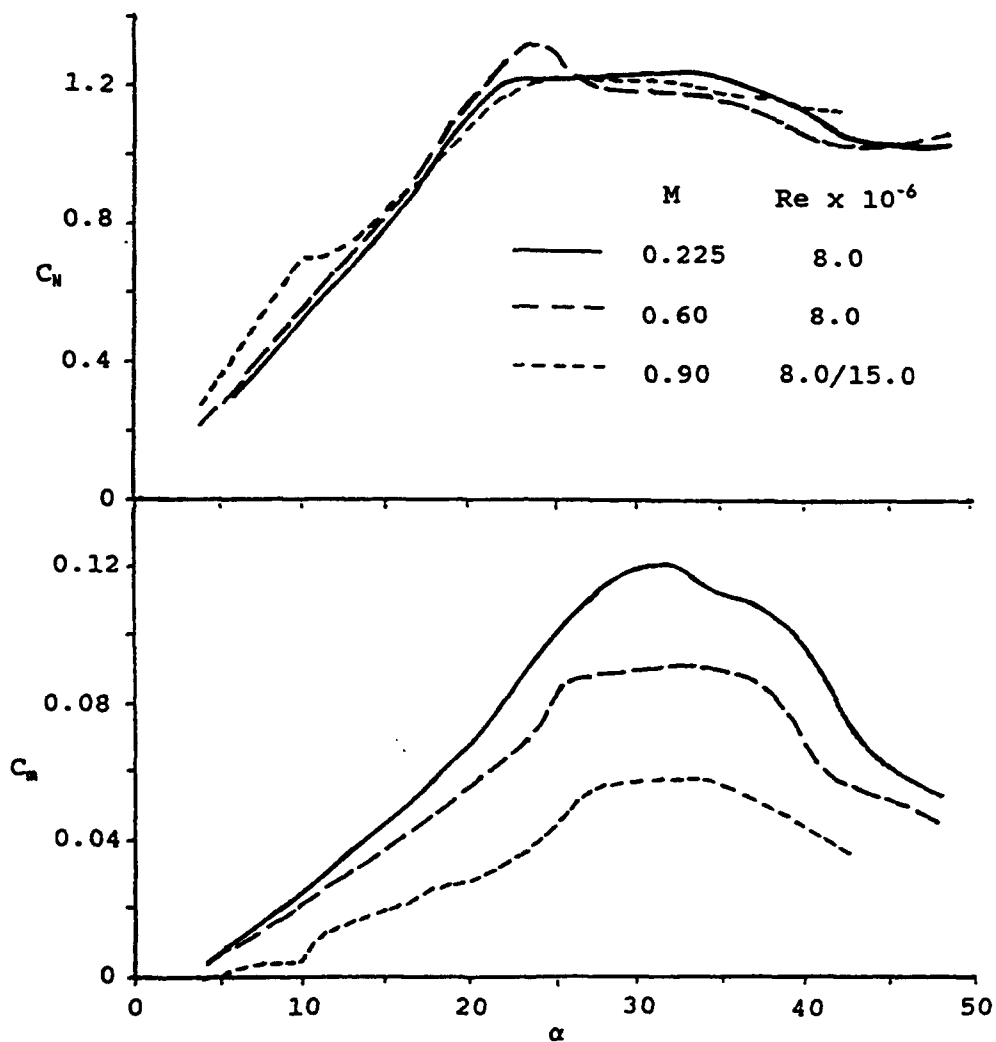


Figure 10 Effect of Mach Number on the Semispan Simple Straked Wing Model C_N and C_m in the NLR HST

test. These analyses provided further insight to the transonic flow phenomena that form the force and moment characteristics that were shown in Figure 10 at $M = 0.9$. The following discussion is a summary of the discussions presented in Reference 11, the purpose of which was to develop a transonic version of Figure 5 that was presented for low speed flow. As stated in Reference 11, the ideas expressed below are preliminary due to the preliminary nature of the data base being discussed.

Normal force, C_N , and pitching moment, C_m , variation with α are shown in Figure 11 for $M = 0.9$ and $R_e = 8 \times 10^6$. These are the mean data for the model oscillating in pitch at ± 0.5 deg amplitude at 6 Hz, and thus are not true "steady" values. By oscillating this model at these fixed dynamic conditions and varying the mean incidence through an α -sweep, static hysteresis effects were avoided. This approach also provided valuable derivative information at each mean incidence.

The trends noted up to 10 deg represent essentially attached transonic flow developments which are dominated by shock systems on the 40 deg swept outer wing panel. Although flow-viz data in Reference 11 indicated the presence of a weak strake vortex beginning at about $\alpha = 6$ deg, this flow feature is not a primary contributor to force and moment developments. The shock system is composed of a forward shock and an aft shock. With increasing incidence, the forward shock sweeps aft until it merges in the wing tip region with the aft shock. This occurrence precipitates the onset of shock induced trailing edge separation (SITES) as is fully discussed in Reference 12.

The onset of SITES signals the beginning of the transition zone which actually starts between $\alpha = 10$ deg and 10.5 deg. Between $\alpha = 10.5$ deg and 11 deg, a second transition occurs in which the three outboard chordwise pressure rows 2, 3, and 4, show leading edge separation onset. Although this double transition seems to be a single one, the same two transitions on the LCO model with a wing tip launcher occur at about 6.5 deg to 7 deg (SITES) and about 9 deg (leading edge separation), respectively.

Once the double transition is complete, vortex flow development becomes the dominant flow feature. The transonic strake vortex seems to have many characteristics in common with the low speed strake vortex. The transonic wing vortex, however, seems to be a combination of forward shock, shock induced separation, leading edge separation, and vortex flow. The vortex system gains strength with increasing α up to about 19 deg where the breakdown process begins.

As was discussed in Reference 11 with regard to results at $\alpha = 19$ deg and 20 deg, the appearance of the new flow structure, "shocklets," and "finger vortices," coincides with a distinct change in pressure data. The fact that maximum suction

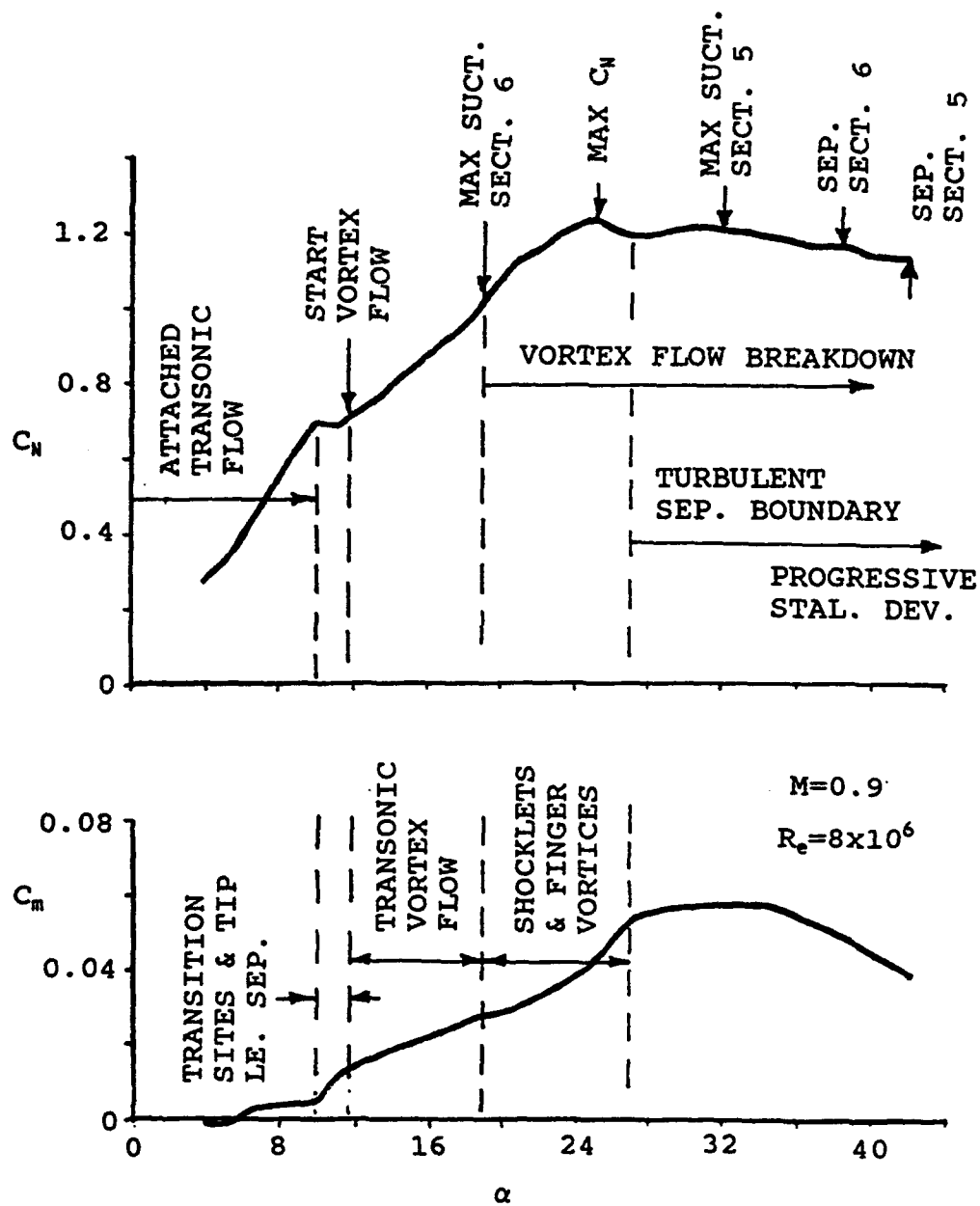


Figure 11 Steady Force and Moment Characteristics for the Simple Straked Wing Semispan Model at $M = 0.9$

corresponding to the wing vortex is achieved at Section 6 at this same angle, indicates that the breakdown process begins with changes in the wing vortex. This makes sense because pressure and flo-viz characteristics of the strake vortex do not show any significant change at this angle. Thus, it appears that the wing vortex is transformed into the shocklet/finger vortex structure at about $\alpha = 19$ deg. Although this new structure does not have the more coherent features of a conventional wing vortex, it is efficient at producing normal force growth at α ; however, it also produces a significant pitch-up trend which increases with α .

The maximum value of C_m occurs at $\alpha = 25$ deg followed by a small but sharp drop at $\alpha = 26$ deg. Except for a steepening of the C_m curve slope above $\alpha = 25$ deg, no change occurs in this region until $\alpha = 27$ deg where the pitch-up trend suddenly disappears. The pressure and flo-viz data at $\alpha = 26$ deg show a uniform drop in suction at pressure row 7 but no significant change in the flow structure at that location. A very noticeable change does occur, however, in the pressure and flo-viz data at $\alpha = 27$ deg. The suction levels drop significantly and the flow structure changes from the shocklet/finger vortex pattern to another new flow structure, the "turbulent separation boundary," along with a sudden growth in the strake vortex cross-section which is indicative of bursting. It appears that this transition at $\alpha = 27$ deg is dominated by bursting of the strake vortex and breakdown of the shocklet/finger vortex structure.

Another peak in C_m occurs at about $\alpha = 32$ deg where the maximum suction level at Section 5 (on the strake) is also reached. This is followed by a gradual reduction of C_m but small variation in C_m until about $\alpha = 35$ deg where C_m begins to drop more rapidly. The range from $\alpha = 32$ deg on is dominated by progressive stalling as is indicated by separation at Section 6 ($\alpha = 38$ deg) and at Section 5 ($\alpha = 42$ deg). This stalling begins at the trailing edge and wing tip and progresses forward and inboard as is indicated by the pressure and C_m data.

Finally, at $\alpha = 42$ deg, the wing is fully stalled according to the available pressure data. It is likely, however, that some vortical flow still exists on the strake forward of Section 5 as is indicated by the C_m trend. As this vortical flow region is moved forward by progressive stalling, C_m will continue to drop until it reaches that value which corresponds to a stable center of lift that is very near the wing geometric centroid.

These characteristics will be further discussed in the following subsections on unsteady force and pressure data obtained in the simple straked wing test.

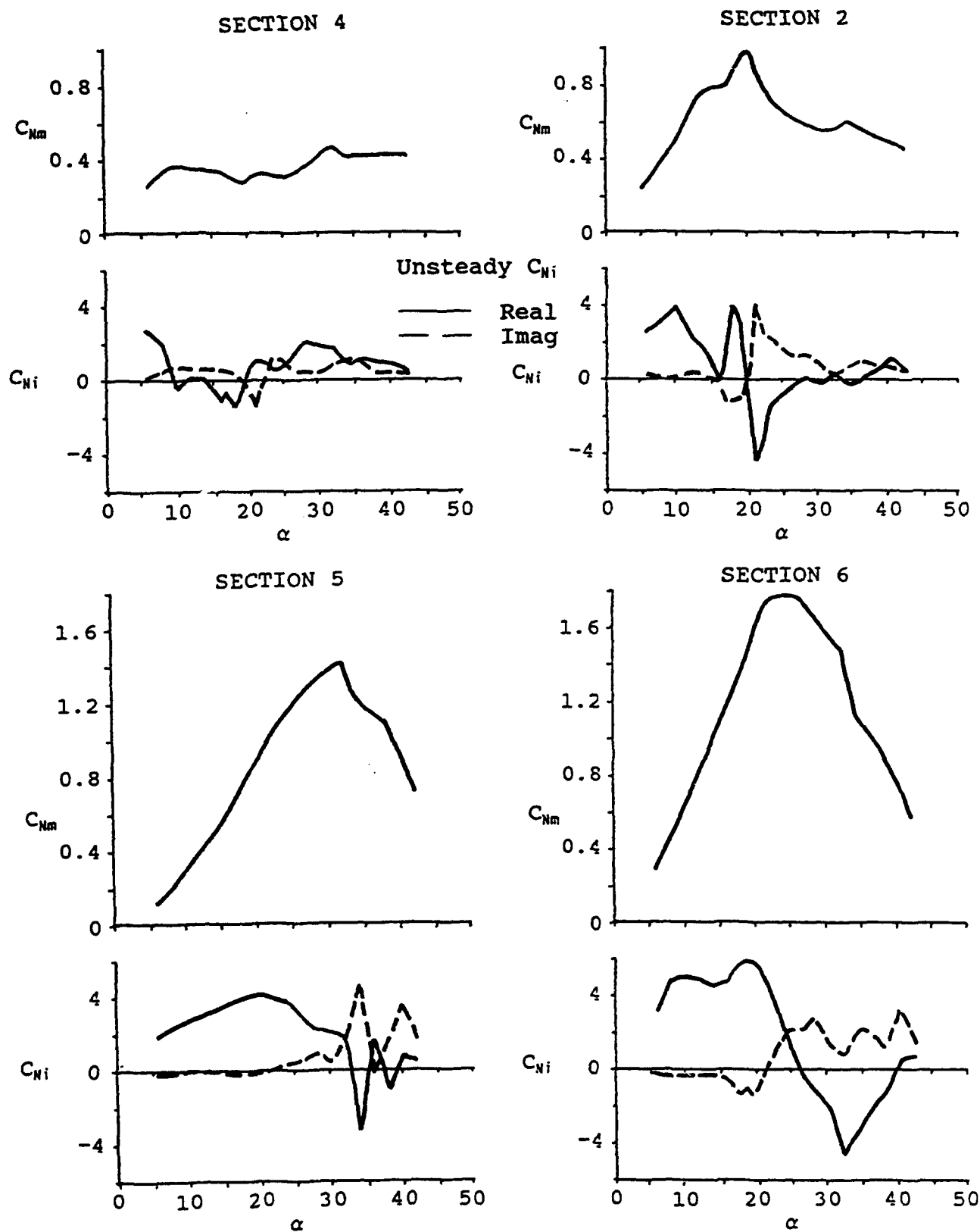
6.5 Small Amplitude Oscillatory Pressure Data

Pressure data obtained at the seven pressure sections on the simple straked wing model provide a more comprehensive view of how flow field conditions on various parts of the wing interact to produce the trends shown in Figure 11. In addition, unsteady results for small amplitude oscillations introduce time varying characteristics which are highly indicative of flow separation transitions as well as other abrupt flow field changes. With 85 pressure transducers located on the wing, however, extensive analysis is needed to determine detailed local trends. A compromise for initial analyses is to examine trends of the integrated pressure section characteristics. A complete set of harmonic results is available for selected data points in Part III of this final report.

Four pressure sections were chosen for this analysis where the variations of mean and oscillatory integrated section normal force characteristics with incidence were examined. Only the upper surface pressure data were used since the primary interest was to better understand the more complicated upper surface flow fields. Two chordwise rows, pressure sections 2 and 4, were chosen to highlight Mach and incidence effects on the development of wing and wing tip flow fields respectively. Two spanwise rows, Sections 5 and 6, were chosen to highlight Mach and incidence effects on vortex flow field developments. With Section 5 being considerably upstream of Section 6, tracking of vortex breakdown progression was possible.

Results are shown in Figures 12, 13, and 14 for the variation of mean and unsteady section normal force coefficients with incidence at $M = 0.225$, 0.6 , and 0.9 , respectively. The unsteady data C_{μ} s are shown as the real or in phase part (solid line) and the imaginary or out of phase part (dashed line). Since the oscillatory frequency was held constant at 5.8 Hz, the reduced frequency was lower at the higher speeds as noted in the figures.

The low speed characteristics shown in Figure 12 for $M = 0.225$ are well known based on extensive analyses conducted on the full span model test data (References 1-6). The trends at Section 4 indicate that the wing tip stalls at about $\alpha = 10$ deg and show little change up to maximum incidence. The more inboard Section 2 results, however, have two distinct peaks where the first at about $\alpha = 12$ deg corresponds to maximum wing vortex lift at that section. The second peak at $\alpha = 20$ deg corresponds to the point at which wing tip stalling has moved inboard of Section 2. The sharp positive spike in the imaginary part of $C_{\mu i}$ at $\alpha = 21$ deg is a typical indicator of an abrupt flow separation point and is also mirrored by a similar but negative spike in the real part of $C_{\mu i}$. After this point, a progressive stalling of the flow at Section 2 occurs up to maximum incidence.



$d\alpha = 0.5^\circ$, $f = 5.8$ Hz, $k = 0.192$, $M = 0.225$

Figure 12 Unsteady Pressure Section Characteristics for Small Amplitude Oscillations, $M = 0.225$

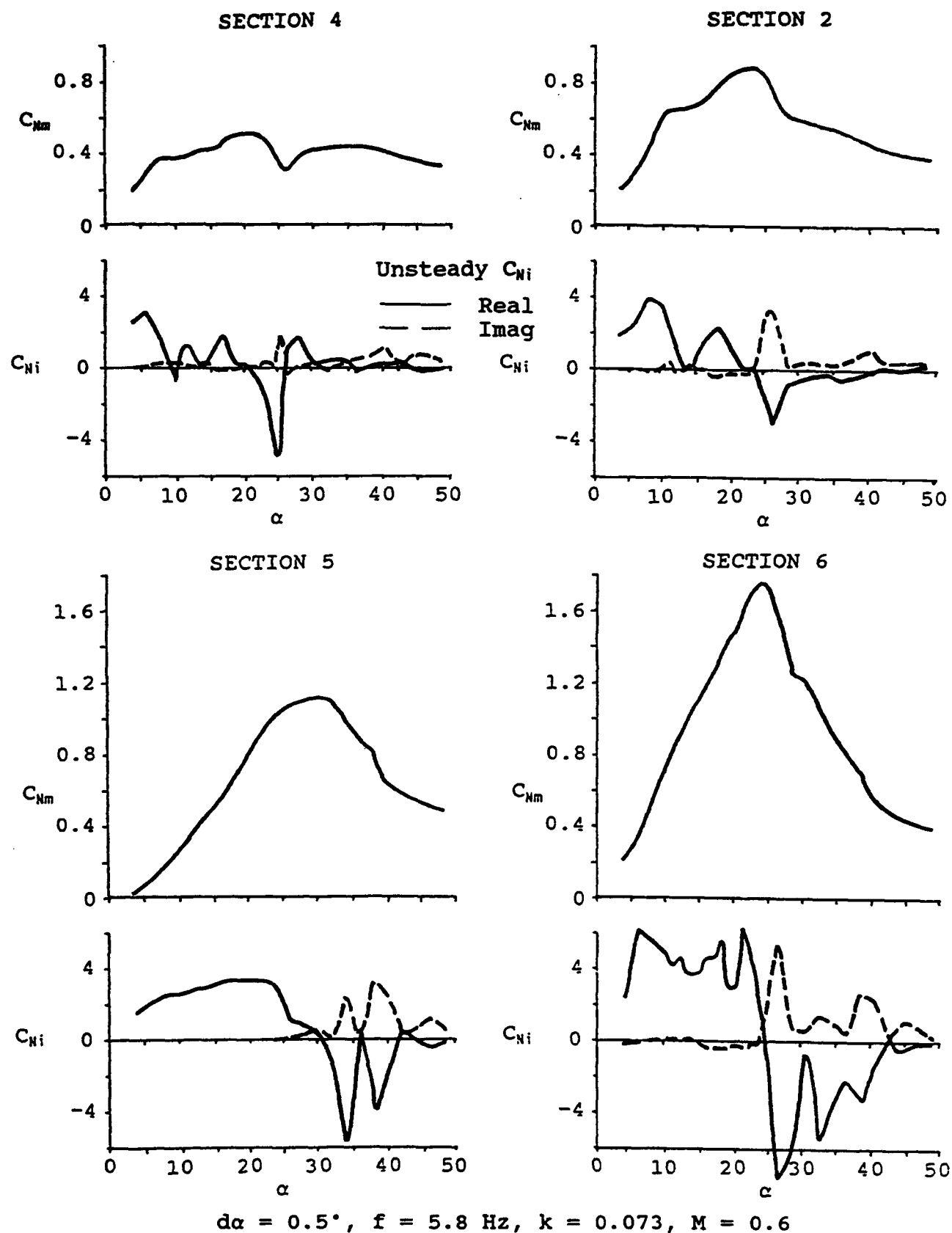


Figure 13 Unsteady Pressure Section Characteristics for Small Amplitude Oscillations, $M = 0.6$

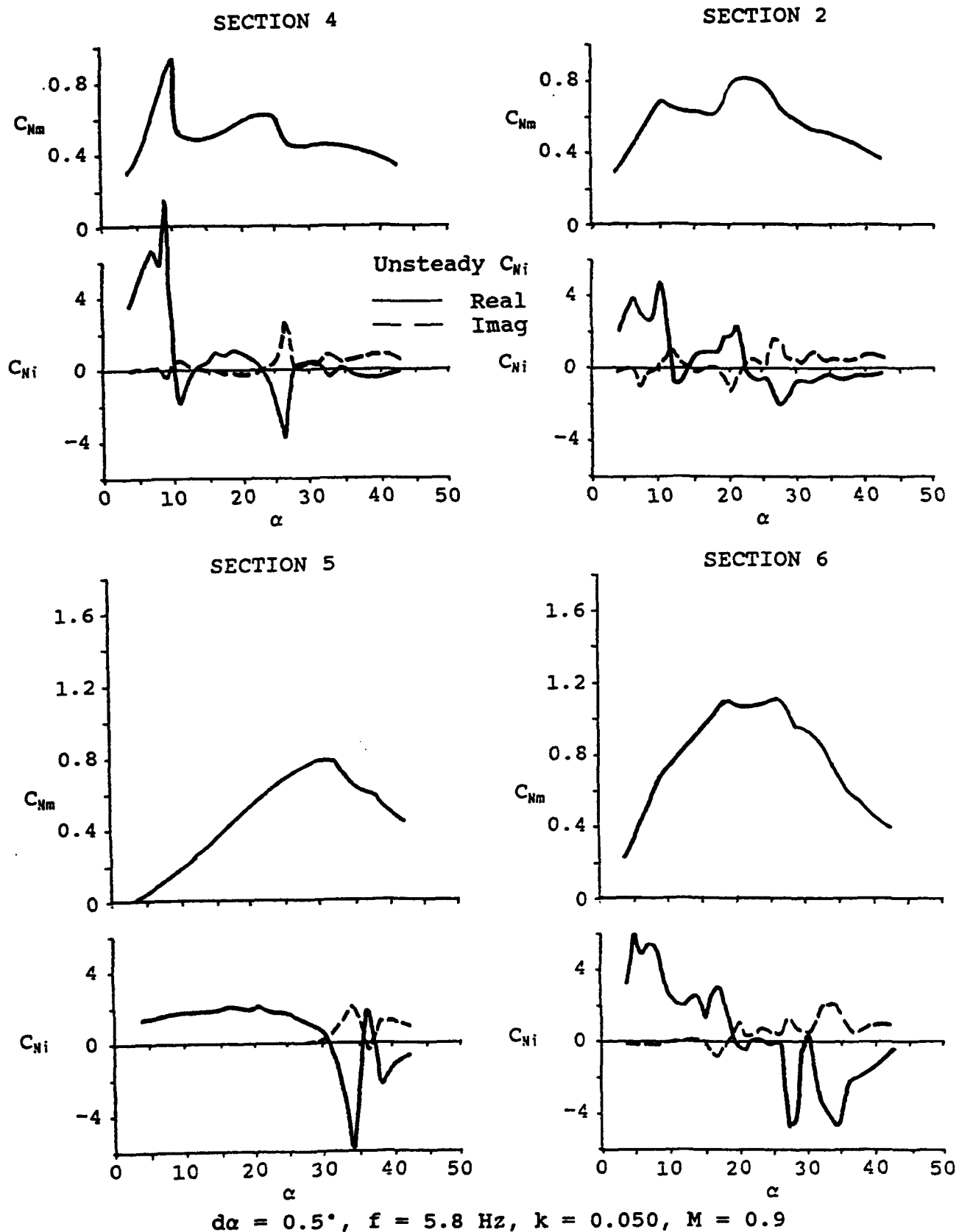


Figure 14 Unsteady Pressure Section Characteristics for Small Amplitude Oscillations, $M = 0.9$

Vortex flow developments on the strake at $M = 0.225$ are classic examples as shown in Figure 12 at Sections 5 and 6. At Section 5 on the strake, vortex lift develops up to $\alpha = 32$ deg after which strake vortex bursting occurs at that section. This is indicated again by the sharp positive and negative spikes in the Imaginary and real parts of C_{Ni} , respectively, at $\alpha = 34$ deg. Since Section 6 is further aft and is affected by both the wing and strake vortices, it shows a clear vortex lift development up to $\alpha = 22$ deg where the wing vortex breakdown begins. Above $\alpha = 26$ deg, the strake vortex also begins to break down at Section 6 which results in a down slope with incidence that starts at 28 deg. Because two vortex systems are involved with the Section 6 flow breakdown process, the sharp spikes noted in C_{Ni} at Sections 2 and 5 do not occur at Section 6. Instead, a general trend of positive imaginary and negative real parts of C_{Ni} exists up to maximum incidence which is more indicative of a progressive flow breakdown and stalling process.

The intermediate speed characteristics are shown in Figure 13 at $M = 0.6$. The trends at Section 4 are different in detail from those at $M = 0.225$ in Figure 12, however, the level is about the same indicating that the wing tip becomes stalled at about $\alpha = 10$ deg. Section 2 also shows similar trends in both C_{Nm} and C_{Ni} as in Figure 12, however, although they occur for the same reasons, the characteristics are not as pronounced. Vortex flow developments at Section 5 are almost identical in both Figures 12 and 13 except that the peak in C_{Nm} is lower and less pronounced at $M = 0.6$. A clear indication of vortical system breakdown at Section 6 is seen in the C_{Ni} spikes at $\alpha = 26$ deg. Although the wing vortex shows signs of breaking down at $\alpha = 23$ deg, the abrupt strake vortex breakdown at $\alpha = 26$ deg is dominant and accelerates the process for the wing vortex. A series of further flow breakdowns also occur at $\alpha = 33$ deg and 39 deg as indicated by spikes in C_{Ni} .

At $M = 0.9$, some distinct changes are seen in the trends as shown in Figure 14. The most notable change is the high lift development on the wing tip at Section 4. This occurs up to $\alpha = 10$ deg and is produced by transonic flows with embedded shocks. This high lift development is terminated by the occurrence of shock induced trailing edge separation (SITES - Reference 12) and leading edge separation. A second but lower peak in C_{Nm} also occurs at $\alpha = 23$ deg to 25 deg which is terminated by a flow separation indicated by peaks in C_{Ni} . This peak is similar to that observed at $M = 0.6$ in Figure 13. Section 2 trends at $M = 0.9$ are surprisingly similar to those seen at $M = 0.6$ both in C_{Nm} and C_{Ni} .

Vortex flow development at Section 5 on the strake at $M = 0.9$ is again very similar to that seen at $M = 0.225$ and 0.6. The vortex lift peak is still lower than that shown for $M = 0.6$ in Figure 13. The developments at Section 6 also indicate a weaker vortex

lift with a significant degradation above $\alpha = 18$ deg which corresponds to the onset of the "shocklets" and "finger vortices" structure discussed in Reference 11. It is obvious that the flow field interactions at this section are quite complicated at $M = 0.9$. Above $\alpha = 25$ deg however, the C_{Nm} and C_{Ni} trends bear a distinct resemblance to those shown at $M = 0.6$ in Figure 13.

The similarities noted in Figures 12, 13, and 14 with Mach number are highlighted in Figure 15 for the mean C_{Nm} results and in Figure 16 for the unsteady C_{Ni} results. In the wing tip region at Section 4, trends for $M = 0.225$ and 0.6 are identical up to $\alpha = 10$ deg whereas the transonic effects are most noticeable for $M = 0.9$. Similarities exist above $\alpha = 10$ deg for $M = 0.6$ and 0.9 , especially around $\alpha = 25$ deg where the C_{Ni} indicate that a flow separation has occurred. The $M = 0.225$ trends are quite different from $\alpha = 10$ deg to 25 deg where they tend to rejoin the $M = 0.6$ trends, especially for the C_{Nm} . Further inboard at Section 2, all three trends for both C_{Nm} and C_{Ni} are very similar where only the magnitude of the peaks or the incidence at which they occur is changed. For instance, the second peak in C_{Nm} occurs at $\alpha = 19$ deg, 23 deg, and 24 deg for $M = 0.225$, 0.6 , and 0.9 , respectively. The separation indicators of positive imaginary peaks in C_{Ni} occur at $\alpha = 21$ deg, 25 deg, and 26 deg for the same conditions, respectively. The peak magnitudes likewise decrease with increasing Mach.

The vortex flow trends at Section 5 on the strake are very similar for both C_{Nm} and especially C_{Ni} . The indications are that with exception of magnitude of the lift, the flow field changes that occur with incidence are virtually identical. Because the strake has a very sharp leading edge with a sweep of 76 deg, this result was expected. Transonic effects take their toll, however, back at Section 6 on the wing. At $M = 0.6$, the development of lift is the same as at $M = 0.225$, but the breakdown after the peak is significantly accelerated. The development at $M = 0.9$ is more rapid at first, similar to what was seen on the wing tip, but breaks abruptly at about 19 deg where vortex flow breakdown onset was identified in Figure 11. Above $\alpha = 26$ deg, the trends for C_{Nm} and C_{Ni} are quite similar for $M = 0.9$ and $M = 0.6$ whereas those for $M = 0.225$ are now out of line. Thus, it appears that at Section 6, the trends for $M = 0.225$ and 0.6 are similar up to $\alpha = 25$ deg and above that angle $M = 0.6$ and 0.9 then become the matching pair. Since $\alpha = 27$ deg was identified as the point for transition to the "turbulent separation boundary" at $M = 0.9$ in Figure 11 (and Reference 11), it is conjectured that a similar flow field transition occurs at $M = 0.6$.

6.6 Large Amplitude Maneuver Force and Moment Data

Results discussed in the previous subsection were obtained with the model oscillating in pitch at a fixed frequency and a small

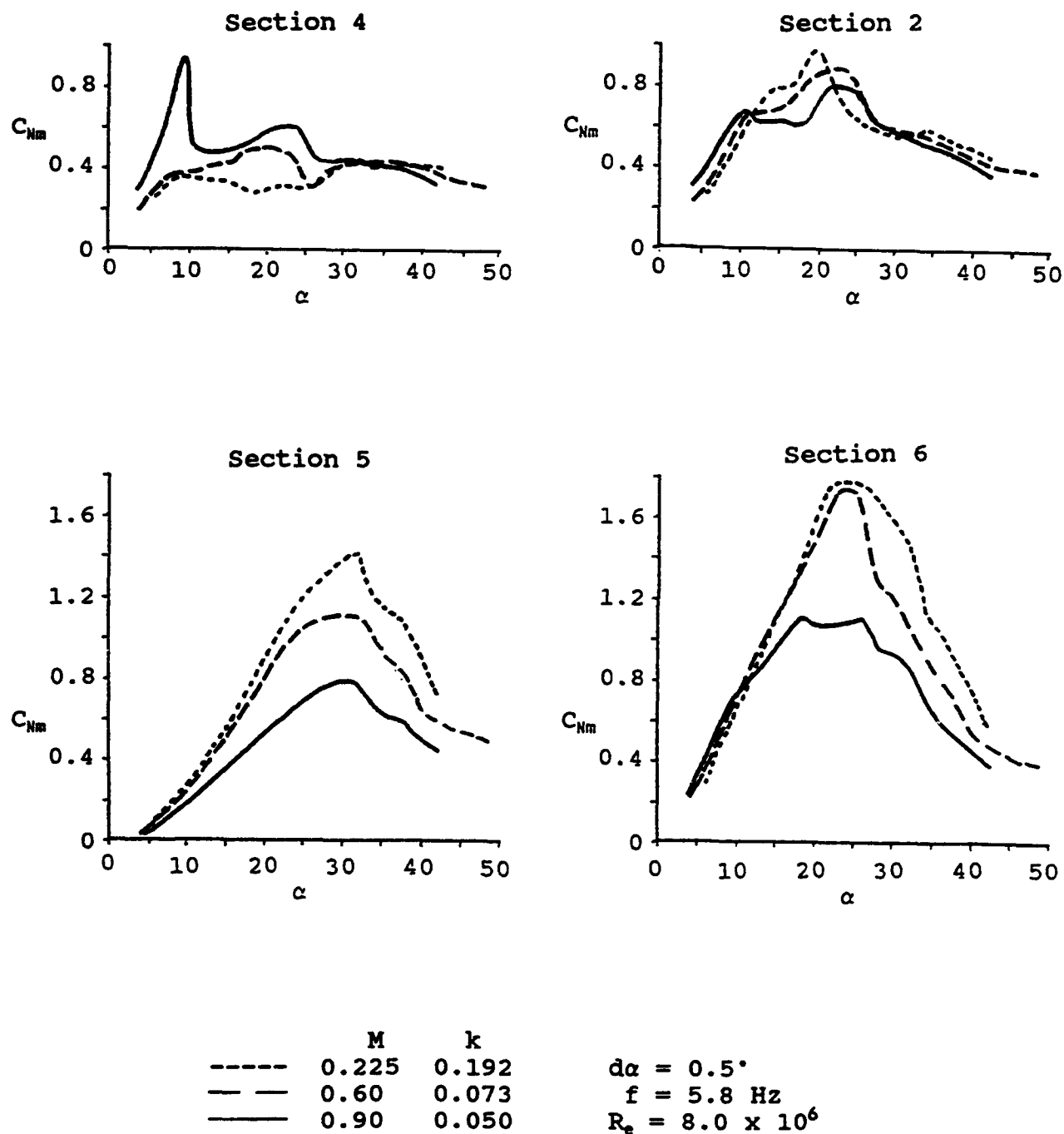


Figure 15 Effect of Mach Number on Mean Pressure Section Characteristics

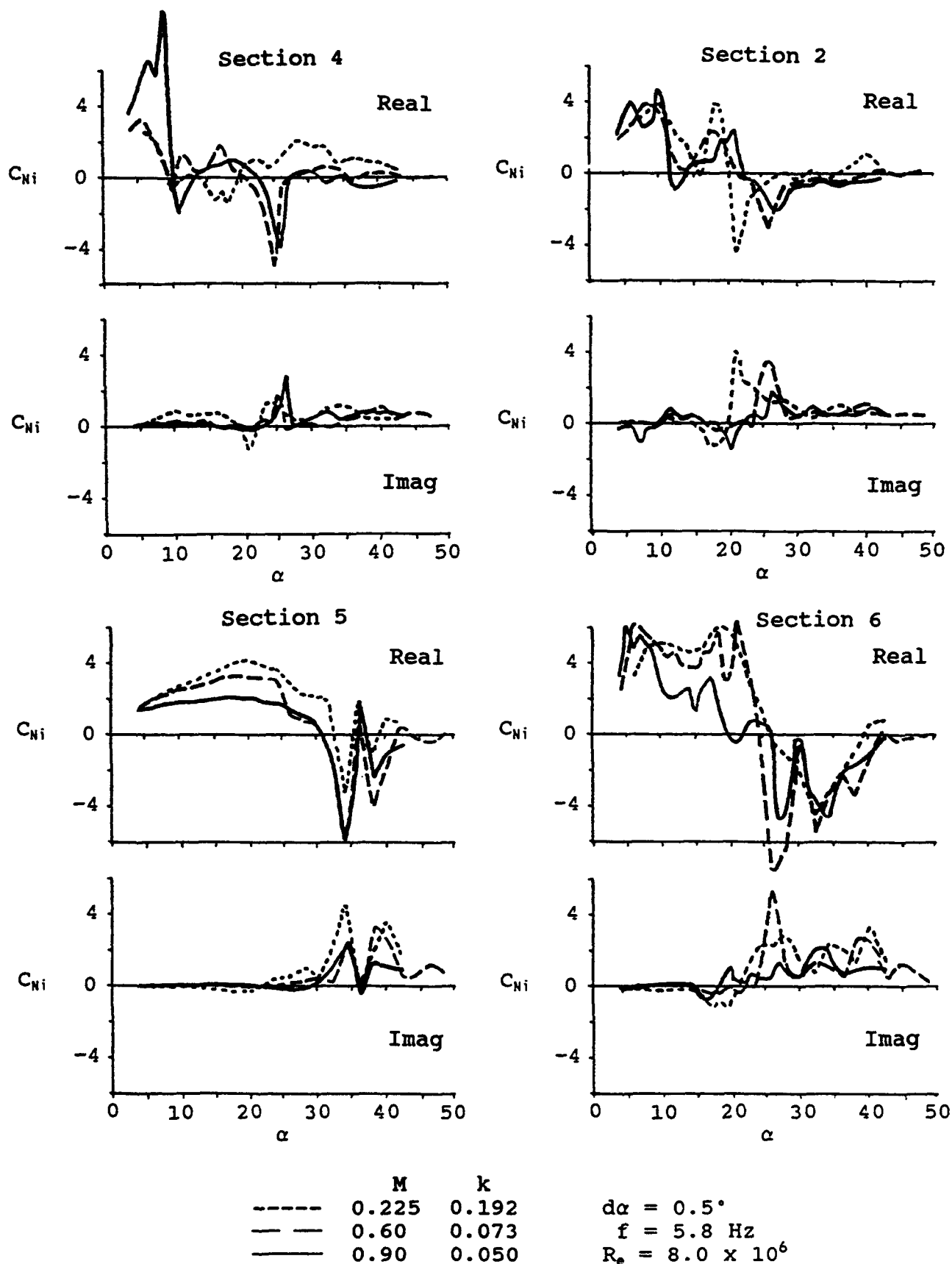


Figure 16 Effect of Mach Number on Unsteady Pressure Section Characteristics

amplitude of 0.5 deg but with a changing mean angle for an α -sweep from 4 deg up to 48 deg. This subsection will present and discuss results obtained with the model performing a single large amplitude motion representative of a pull-up/push-over maneuver in flight. The period for this maneuver is 0.26 sec (3.8 Hz) in the wind tunnel test which for a 1/9-scale model would increase to 2.37 sec for a full scale maneuver. In these data, the effects of maneuver time history are important where as they were not in the small amplitude cases discussed previously. The most obvious time history effect is the lag time required for a given flow transition to occur. This lag time is also a function of the flow condition from which the transition is occurring. Quite simply, it takes longer for a flow field to reattach from a separated flow than for it to separate from an attached flow. This is because flow field information propagates more readily in an attached flow than in a chaotic separated flow. An exception is where leading edge separation rolls up into a vortex on a highly swept leading edge. Much more discussion on these phenomena is given in References 2 through 6. Also, a complete set of time history results for selected maneuver data points is available in Part IV of this final report.

The variation of C_N and C_m with incidence and pitch direction is shown in Figure 17 at $M = 0.225$. The pitch up begins at $\alpha = 7$ deg, stops and begins pitch down at $\alpha = 37$ deg and stops pitch down back at $\alpha = 7$ deg. The time history variation of α is a (1-cos) wave form which is representative of dynamic pull-up/pushover maneuvers in flight. (This is also similar to the "Pugachev Cobra" maneuver as discussed in more detail in Reference 13.) The time varying data are shown as a solid line for pitch-up and a dashed line for pitch down in a hysteresis loop. Static mean data are shown as dotted lines for reference.

On pitch up, both C_N and C_m tend to follow the static data but overshoot where static vortex breakdown occurs. This breakdown is delayed primarily by the lag time required for it to occur. On pitch down, the flow fields catch up and become more separated than in the static case because of the initial lift overshoot. The flow remains separated to an angle below the burst point where it rejoins the static data once the transients have died out. Pitching moment is more sensitive to pitch down at the lower angles (below $\alpha = 18$ deg) where the dynamic characteristic is more nose up all the way down to the initial angle.

The same maneuver was repeated at $M = 0.6$ for which the dynamic C_N and C_m results are shown in Figure 18. A similar trend is seen as was shown in Figure 17 for $M = 0.225$. Shapes of the dynamic hysteresis loops are somewhat different where the $M = 0.6$ data are more indicative of a lower reduced frequency for the maneuver (or a larger nondimensional maneuver period) because of the higher velocity.

At $M = 0.6$, the characteristics are quite different if the same maneuver starting angle is increased from 7 deg to 15 deg as

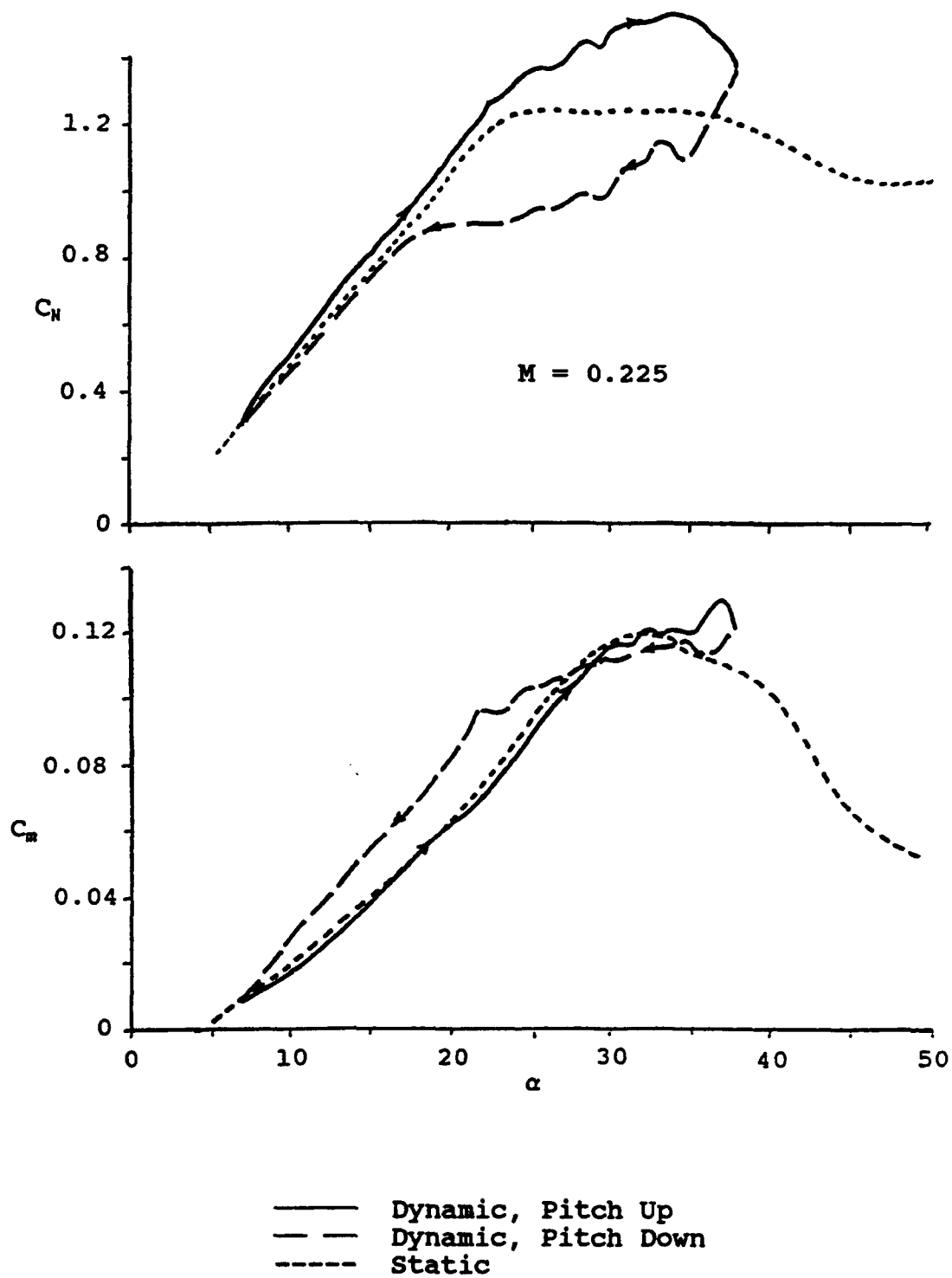


Figure 17 Pitch Up/Push Over Maneuver Motion Between $\alpha = 7^\circ$ and $\alpha = 37^\circ$ for $M = 0.225$

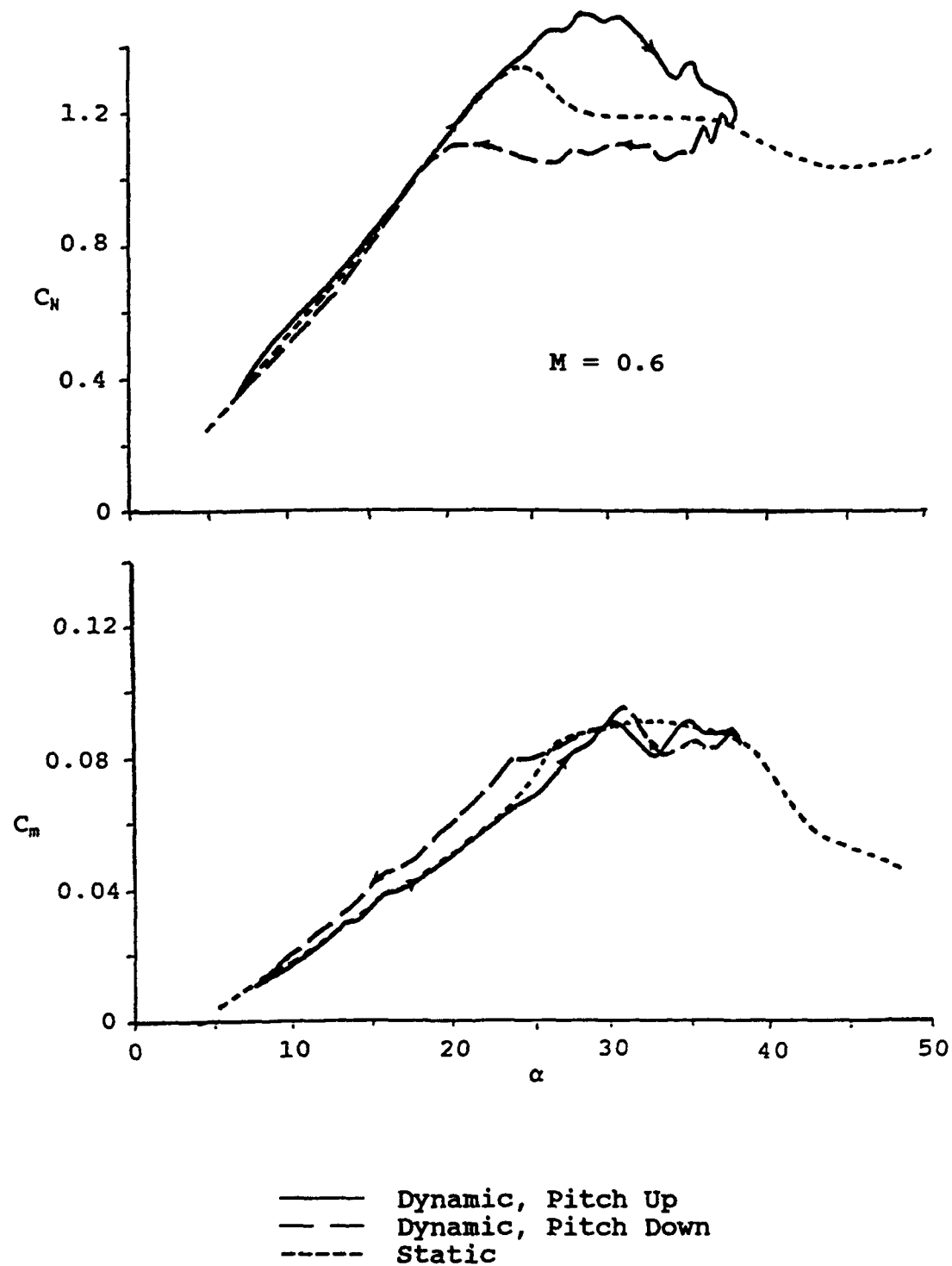


Figure 18 Pitch Up/Push Over Maneuver Motion Between $\alpha = 7^\circ$ and $\alpha = 37^\circ$ for $M = 0.60$

shown in Figure 19. Because most of the maneuver is taking place in flow fields that are dominated by either vortex breakdown or stalling, the hysteresis loops are much more pronounced. Also, even through the nondimensional maneuver time is much longer at $M = 0.6$, the hysteresis loops are more dynamic than those shown at $M = 0.225$ at the lower incidence range in Figure 17. A comparison of Figures 17, 18, and 19 vividly demonstrates how flow transition lag times increase with increasing deterioration of the flow fields.

Returning to the original incidence range of $\alpha = 7$ deg to 37 deg and increasing Mach to 0.9 yields yet still another variation of the hysteresis loops as shown in Figure 20. Overall, the hysteresis loops at $M = 0.9$ are narrower than those shown in Figure 18 for $M = 0.6$ because of a further increase in the nondimensional maneuver time at the higher speed. As noted in Figure 20, there seems to be two regimes where the characteristics above $\alpha = 20$ deg are more like those shown in Figures 17 and 18. It is suspected that this incidence range is dominated by vortex breakdown and stalling processes as discussed in Reference 11. Therefore, the trends shown in Figure 20 for $\alpha > 20$ deg seem reasonable.

Below $\alpha = 20$ deg in Figure 20, a very different trend is seen where the hysteresis characteristics are not symmetrical about the mean flow data. A significant delay in the breakdown at $\alpha = 10$ deg is seen for pitchup but very little delay is seen in flow reestablishment on pitch down. This is opposite to the usual trend where the lag time for flow breakdown is much less than that for flow reestablishment. The small delay for pitch down agrees with the conclusions based on Figure 14 that mild hysteresis should exist around $\alpha = 10$ deg to 11 deg as indicated by small positive peaks in the imaginary parts of C_{Ni} at Sections 2 and 4. The large delay for pitch up is not explainable at this time. However, since no hysteresis tendency around $\alpha = 10$ deg is noted at Sections 5 and 6 in Figure 14, the aerodynamic lag would be expected to be confined to the wing tip region for $\alpha < 20$ deg.

Since the hysteresis below $\alpha = 20$ deg in Figure 20 is most likely controlled by wing tip flow field transitions, then the asymmetry must be associated with those processes. As discussed earlier in this section and in Reference 11, the dominant flow transitions around $\alpha = 10$ deg on the simple strake wing tip region at $M = 0.9$ are SITES and leading edge separation. Thus, the implications of Figure 20 are that these flow transitions are sensitive not only to the magnitude of pitch rate but also its direction. Furthermore, the effect of direction appears to be dominant for rates above some unknown threshold. The character of these interactions can be determined by a careful analysis of the time history development of the four wing tip pressure section distributions. These data exist as part of the data base developed from the simple straked wing test.

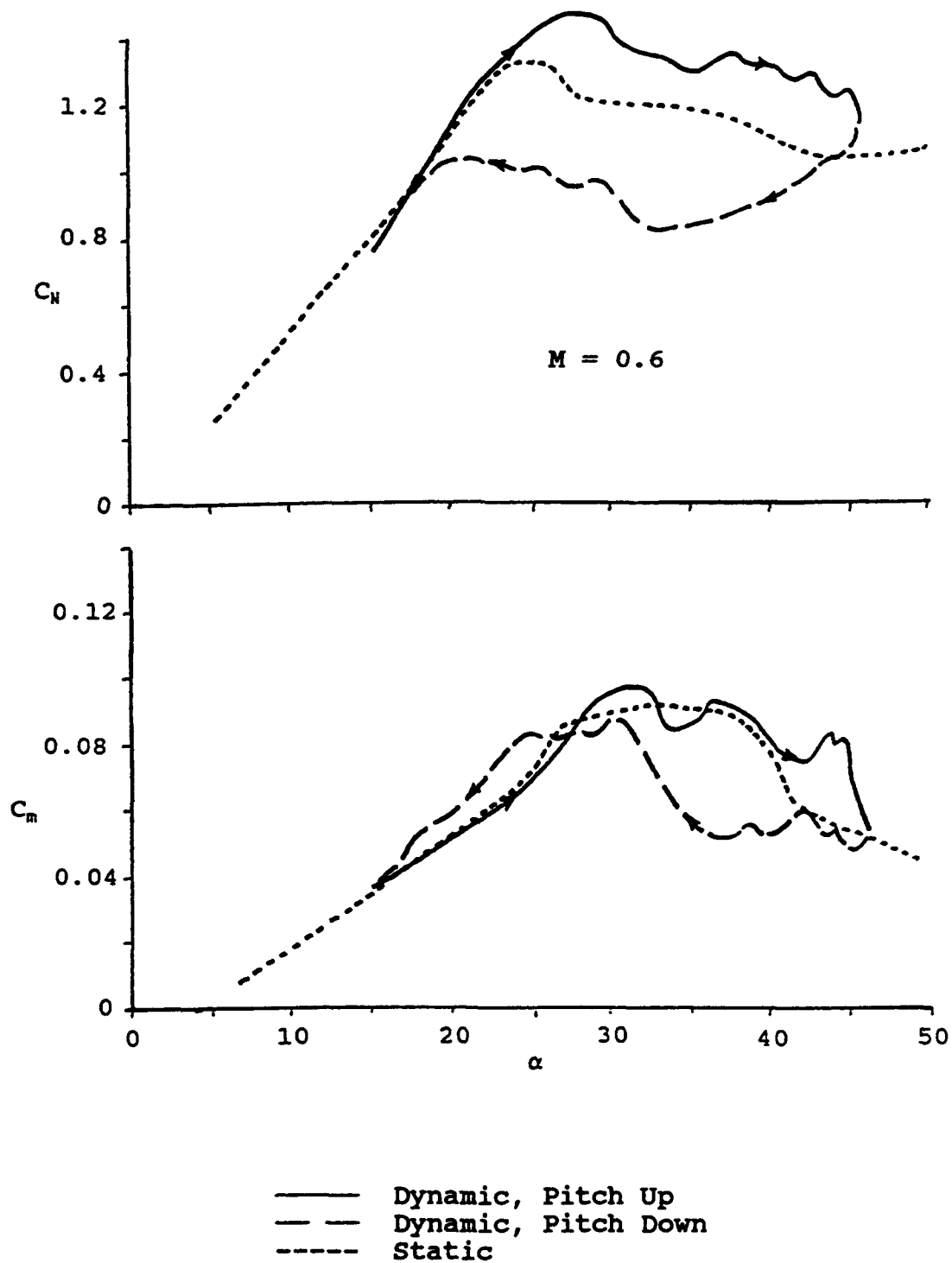


Figure 19 Pitch Up/Push Over Maneuver Motion Between $\alpha = 15^\circ$ and $\alpha = 45^\circ$ for $M = 0.60$

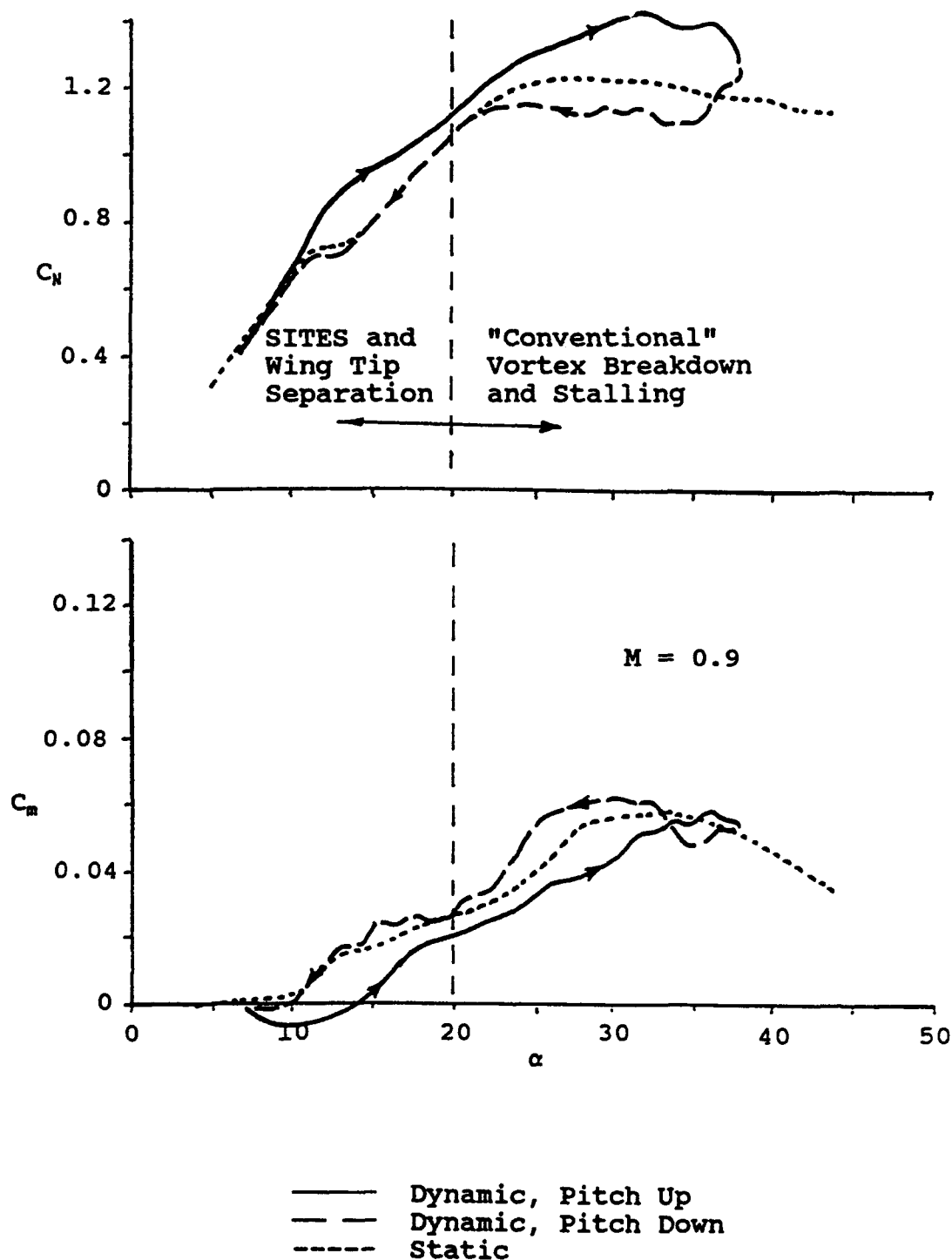


Figure 20 Pitch Up/Push Over Maneuver Motion Between $\alpha = 7^\circ$ and $\alpha = 47^\circ$ for $M = 0.90$

7.0 CONCLUDING REMARKS

A wind tunnel investigation was conducted in May of 1992 to investigate the unsteady aerodynamic aspects of transonic high incidence flows over a simple straked wing model. This test was designed to show how low speed vortex type flows evolve into complicated shock vortex interacting flows at transonic speeds. Requirements for this test were based on a low speed test conducted in 1986 on a full span model in the NLR Low Speed Tunnel. The transonic model was a semispan version of the low speed model with some modifications. It was equipped with a three-component semispan balance to measure total wing loads, seven rows of high response pressure transducers to measure unsteady pressures and 15 vertical accelerometers to measure model motion and vibrations. The model was oscillated sinusoidally in pitch at various amplitudes and frequencies for mean model incidences varying from 4 deg to 48 deg. In addition, maneuver type transient motions of the model were tested with amplitudes of 16 deg and 30 deg total rotation at various starting angles. The test was conducted in the NLR HST in the Mach range of 0.225 to 0.90 with some preliminary vapor screen flow visualization data taken at $M = 0.6$ and 0.9 . More details of this model and test are provided in Part II of this final report.

A significant data base obtained which included at the three Mach numbers: mean incidence variations of either 1 deg or 2 deg increments; amplitude variations from 0.5 deg to 8.0 deg; frequency variations from 5.7 Hz to 15.2 Hz; and transient maneuvers. Preliminary flow visualization data were also obtained from a limited test in which a laser light sheet/water vapor technique with a high speed video recording system at up to 1000 frames per second was used.

Correlations of steady pressure and force data from the HST test with those from the 1986 LST test at equivalent flow conditions showed that the transonic test set up was a good representation of the low speed test. Since the transonic model was a semispan model, wall clearance was varied where it was determined that the smallest clearance gave the best results. All major flow field transitions were duplicated between the two tests, however, the incidences at which each occurred varied slightly.

Steady normal force and pitching moment variations with incidence were used to demonstrate the overall effects of Mach number for $M = 0.225$, 0.6 , and 0.9 . Results from the analyses of the force, pressure, and flow visualization data conducted under a separate study, were used to further describe the transonic flow phenomena believed to exist over the straked wing for incidences ranging from 4 deg to 42 deg at $M = 0.9$.

Pressure data from small amplitude oscillatory test runs were analyzed to provide additional insight into flow field evolution with increasing Mach number. Using integrated pressure section normal force coefficients for two wing tip chordwise rows and two strake spanwise rows, wing and strake vortex flow interactions were examined. It was found that transonic effects on the wing tip flows were very pronounced at lower incidences but were less so at higher incidences. Strake vortex flows seemed to show little change of character with Mach number but did show a substantial reduction in vortex lift as Mach approached 0.9.

Unsteady normal force and pitching moment time histories for transient pitch up/push over maneuvers also showed a definite effect of increasing Mach number. Since the maneuver time was maintained constant (as representative of full scale aircraft maneuvering) unsteady effects decreased as speed increased. This was attributed to an increase in the nondimensional maneuver time which varies directly with velocity. Data at $M = 0.9$ showed similar characteristics as those for $M = 0.225$ and 0.6 at the higher incidences, however, at lower incidences the characteristics were quite different and unexpected. Although no explanation for this anomaly was offered, sufficient data are available from the test to answer these questions.

8.0 REFERENCES

1. Cunningham, A.M., Jr., den Boer, R.G., et al: Unsteady Low-Speed Wind Tunnel Test of a Straked Delta Wing, Oscillating in Pitch, AFWAL-TR-87-3098 (Parts I through VI), April 1988.
2. den Boer, R.G. and Cunningham, A.M., Jr.: "Low Speed Unsteady Aerodynamics of a Pitching Straked Wing at High Incidence - Part I: Test Program," Journal of Aircraft, Vol. 27, January 1990, pp. 23-30.
3. Cunningham, A.M., Jr. and den Boer, R.G.: "Low Speed Unsteady Aerodynamics of a Pitching Straked Wing at High Incidence - Part II: Harmonic Analysis," Journal of Aircraft, Vol. 27, January 1990, pp. 31-41.
4. Cunningham, A.M., Jr.: "A Critique of the Experimental Aerodynamic Data Base for an Oscillating Straked Wing at High Angles," Proceedings Fourth Symposium on Numerical and Physical Aspects of Aerodynamic Flows, California State University, Long Beach, California, 16-19 January 1989.
5. Cunningham, A.M., Jr., and den Boer, R.G.: "Steady and Unsteady Aerodynamics of a Pitching Straked Wing Model at High Angles of Attack," presented at the AGARD FDP Symposium "Vortex Flow Aerodynamics," Scheveningen, The Netherlands, 1-4 October 1990.
6. Cunningham, A.M., Jr., and den Boer, R.G.: "Analysis of Unsteady Force, Pressure and Flow-Visualization Data for a Pitching Straked Wing Model at High Angles of Attack," presented at the AGARD FDP Specialists' Meeting "Maneuvering Aerodynamics," Toulouse, France, 1-2 May 1991.
7. den Boer, R.G. and Cunningham, A.M., Jr.: "Unsteady Transonic Wind Tunnel Testing of Fighter Type Wings," 31st AIAA/ASME/ASCE/AHS/ASC Structures, Structural Dynamics, and Materials Conference, Long Beach, California, April 2-4, 1990.
8. Cunningham, A.M., Jr., and den Boer, R.G.: "Transonic Wind Tunnel Investigation of Limit Cycle Oscillations on Fighter Type Wings - Update," AIAA Dynamics Specialist Conference Proceedings, Dallas, Texas, 16-17 April 1992.
9. den Boer, R.G.: "Application of the New NLR Measurement System PHARAO in Unsteady Wind Tunnel Tests on Straked Delta Wings," presented at the 18th ICAS Congress, Beijing, China, 20-25 September 1992.

10. Poestkoke, R., "Hydraulic Test Rig for Oscillating Wind Tunnel Model," National Aerospace Laboratory, Amsterdam, The Netherlands, NLR MP 76020 U, 1976.
11. Cunningham, A.M., Jr.: "A Preliminary Assessment of the Transonic Aerodynamic Characteristics of a Straked Wing Configuration," Lockheed Fort Worth Company, July 1993.
12. Cunningham, A.M., Jr., and Spragle, G.S.: "A Study of the Effects of Reynolds Number and Mach Number on Constant Pressure Coefficient Jump for Shock Induced Trailing-Edge Separation," NASA CR 4090, August 1987.
13. Cunningham, A.M., Jr. and Bushlow: "Steady and Unsteady Force Testing of Fighter Aircraft Models in a Water Tunnel," AIAA Paper No. AIAA-90-2815, August 1990.